What to do with CO2?

Towards valuable chemicals using plasma and catalysis

Ronda Lloret, M.

Publication date
2021

Chapter 1

Introduction

Converting CO_2 into valuable chemicals

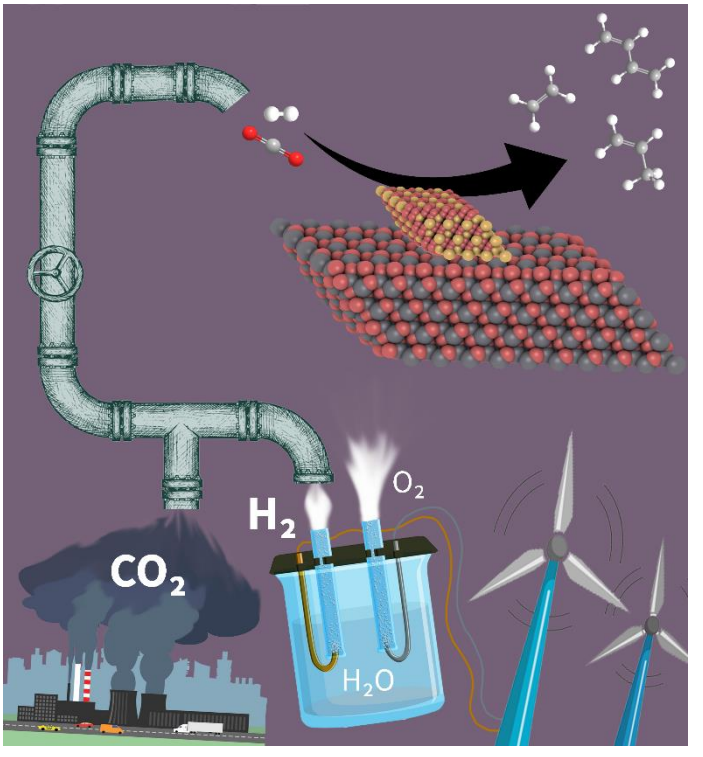

Part of this work has been published as: 'A Critical Look at Direct Catalytic Hydrogenation of Carbon Dioxide to Olefins', M. Ronda-Lloret, G. Rothenberg and N. R. Shiju, *ChemSusChem.*, **2019**, 12, 3896–3914.

The increasing amount of anthropogenic carbon dioxide (CO_2) emissions is a global concern. There is a correlation between the rise in global temperatures and the rise in atmospheric CO_2 concentration levels (Figure 1.1).[1] Even if this does not imply direct causality, mankind cannot afford to take chances. This feeling is echoed in the 2015 Paris Agreement, which shows the willingness of policy experts, scientists and climate economists from 118 countries to take measures for fighting climate change. Its main goal is keeping the increase in the global average temperature below 2 °C and ultimately achieving net-zero emissions of greenhouse gases (GHGs).[2,3]

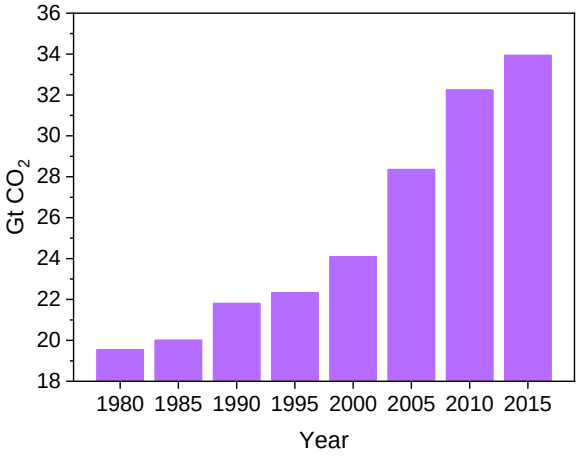

Figure 1.1. World CO_2 net emissions from 1980 to 2015.[4]

This goal is feasible, yet difficult. Reducing the amount of CO_2 in the atmosphere could reduce the greenhouse effect, but this requires individuals and companies to change their behaviour. This requires economic and social incentives, such as controlling the 'carbon footprint', higher taxes on carbon emissions or on fossil fuels. The main sources of CO_2 emissions are power generation and manufacturing (Table 1.1). Heavy industry, residential heating, cooking, and road transport are the heaviest energy consumers, and this energy comes mainly from fossil fuels.[4] Moving away from fossil fuels to cleaner energy sources remains a big challenge, partially due to the large volumes of fossil fuels that are consumed and available today. The total reserves of fossil fuels were >900 billion tonnes of oil equivalent (toe) in 2015.[5] This means that, at the current

consumption, there are enough available fossil fuels at least for another 100 years.

Developed countries are starting to act in terms of renewables and natural gas, bringing down emissions. For example, according to the European Environmental Agency (EEA), Europe avoided the emission of 460 Mt of CO_2 in 2016 by the use of renewable energy.[6] The main renewable energy sources are onshore and offshore wind power and solar photovoltaics for electricity generation, as well as solid biomass-based technologies for heating and cooling.[6,7] In addition, the EU remains a world leader in renewable power, with 0.87 kW of renewable energy capacity installed per person in 2017, followed by the United States (0.71 kW/person) and Brazil (0.61 kW/person).[6] Nevertheless, the use of coal and its technology remains well established. In 2017, a net capacity of 35 GW from burning coal was added to the global fleet.[6] The gross addition was 67 GW (mainly in developing economies) and the capacity retired was 32 GW (mainly in the United States and Europe).[6]

Table 1.1. Total CO_2 emissions by sector in 2015.[4]

Sector	CO_2 source	Percentage of world energy consumption	Emissions (Gt)
Electricity	Carbon-based power plants	22.0	12.4
Heavy industry	Production of cement, limestone and hydrogen	17.2	3.9
Transport	Road > air > ship > rail	21.9 > 3.1 > 2.8 > 0.6	6.0 > 0.9 > 0.8 > 0.1

In fact, if we examine regions under fast economic development, such as South-East Asia, we see that coal usage is increasing, especially with the commissioning of numerous coal-fired power plants since 2000.[3,8] Examining the magnitude and the distribution of the world energy demand, it looks like coal, oil and natural gas will remain our main energy sources in the coming 50

years. Changing this large-scale trend is possible only through a combination of economically viable alternatives and strong regulations.

Scientists have been studying methods for reducing CO_2 emissions for decades. Capturing CO_2, either from flue gases of industrial processes or directly from the atmosphere, is one such option. Yet carbon capture and storage (CCS) presents technical and economic barriers. CO_2 leakage rates are uncertain and there are limits in the storage capacity depending on the location. Moreover, CCS requires strong regulatory incentives since it does not produce any intrinsic value.[9] Perhaps the strongest argument against CCS, however, is that it basically considers CO_2 as garbage. This is not a good chemical solution. Instead, **we should consider CO_2 as a resource**, aiming at carbon capture and utilization (CCU). If we could use CO_2 as raw material to make profitable products, governments and companies would be encouraged to follow this. The basic technology is already taking place, using the absorption of CO_2 in solvents such as monoethanolamine (MEA) to give carbamates (Figure 1.2).[9] During post-combustion capture, flue gases including CO_2 are bubbled through a MEA solution. The CO_2 is then recovered by heating the carbamate solution.[10] Afterwards, the CO_2 is cleaned (and dried if necessary) and compressed for transport and utilisation. This method still has drawbacks regarding the energy penalty of the MEA regeneration process. Other amine solvents are being researched, as well as physical adsorption processes using solid adsorbents such as activated carbons, molecular sieves, zeolites and polymers, among others.[11]

After capture or separation of CO_2, efforts are being done to efficiently convert CO_2 into high value-added products such as fuels and chemical feedstock. Converting CO_2 to urea (for fertilizers) and the production of plastics such as polycarbonates are done today.[3,12] Methanol synthesis is industrially obtained from a mixture of CO_2, CO and H_2.[13] However, methanol is nowadays also obtained from CO_2. For example, Carbon Recycling International developed the world's first commercial CO_2 to methanol plant in Iceland. The so-called George Olah Renewable Methanol Plant recycles now 5.5 ktons of carbon (albeit that this was done in Iceland, where renewable energy is abundant).[14]

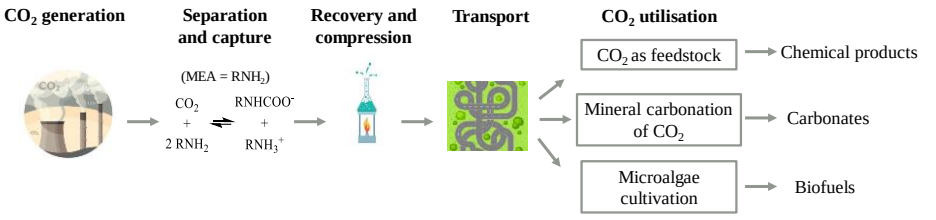

Figure 1.2. Scheme of CO_2 capture by absorption in monoethanolamine (MEA), and different CO_2 utilisation options.

However, to use CO_2 in any chemical process we must overcome its high thermodynamic stability, as its $\Delta G^0 = -394.4$ kJ mol^{-1}, which usually means high reaction temperatures. One way of reducing the energy penalty of CO_2 conversion is by using a high energy co-reactant.[12] For this purpose, hydrogen ($\Delta G^0_{(H2)}$ = 0.0 kJ mol^{-1}) and *n*-butane ($\Delta G^0_{(n\text{-}C4H10)}$ = -16.57 kJ mol^{-1}) are good candidates.

To lower the activation barrier of the reaction and speed it up we use catalysis. Catalytic CO_2 conversion to high value-added chemicals can be done by different methods. The electrocatalytic pathway has mainly focused on the CO_2 reduction reaction (CO_2RR) to hydrocarbons, as well as to CO and alcohols. This process is already at a higher technology readiness level, but its economic viability depends strongly on the cost of electricity.[15] Another alternative is photocatalysis, typically using semiconductor catalysts, which can enable a direct solar to fuel conversion. While photocatalysis is independent of an electricity source, its efficiency is still too low for large-scale applications.[16] Plasma and plasma-catalytic reactions are also gaining attention, especially CO_2 splitting and dry reforming of methane (DRM).[17–19] Thermocatalytic CO_2 conversion is also well known. For instance, DRM using CO_2 is used to produce syngas, which is then used for the production of hydrocarbons or alcohols through the Fischer-Tropsch synthesis (FTS).[17]

In this work, we study the thermal-catalytic and plasma-catalytic conversion of CO_2 to high value-added chemicals. We use H_2 or *n*-butane as co-reactants. By changing parameters such as reaction temperature, reactants ratio and catalyst, different reactions can take place (Figure 1.3). CO_2 and H_2 can react in the reverse water-gas shift (RWGS, which produces CO and H_2O) or in the hydrogenation of CO_2 to methanol. In combination with *n*-butane, the dry

reforming of butane to obtain syngas, and the oxidative dehydrogenation of butane to butenes and butadiene can take place. In addition, plasma-catalysis is able to dissociate CO_2 to CO.

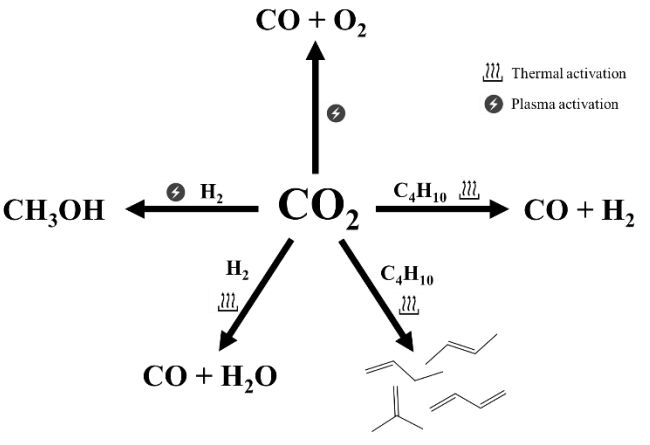

Figure 1.3. CO_2 conversion reactions studied in this thesis.

1.1. CO_2 and H_2

CO_2 hydrogenation will ideally use hydrogen produced from a clean source. Currently, hydrogen is obtained from steam methane reforming (SMR). This process requires (natural) methane gas as a feedstock and emits CO_2, which does not help alleviating CO_2 emissions.[20] Water electrolysis is the main sustainable route for producing hydrogen, provided that renewable energy is used to do so. Renewable energy is mainly obtained from wind power, hydropower and solar photovoltaics, or from excess of electrical energy from non-carbon-based sources (geothermal energy and nuclear power plants during the night).[21,22] One of the main drawbacks of using renewable energy is its storage, because the demand of electricity is not constant in time. While the storage of this energy in batteries or electric grids is under development, the production of H_2 with the surplus of energy from renewable electric plants will help alleviating the storage problem. Other major drawbacks are the current high cost of renewable energy, which translates into high costs on the production of renewable H_2, and safety issues regarding H_2 storage.

CO_2 hydrogenation is a versatile reaction for the valorisation of carbon dioxide. One can alter the reaction parameters (CO_2/H_2 ratio, temperature and pressure), and the catalyst composition (Cu, Ga and noble metal based catalysts, among others) to control the product distribution.[23] Depending on these factors, a wide range of chemical building blocks and high-value-added chemicals can be produced, including carbon monoxide (CO), methane (CH_4), methanol (CH_3OH), ethanol (C_2H_5OH) and lower olefins ($C_2^=$–$C_4^=$).

CO is an important chemical feedstock because it is a basic building block for a variety of important chemicals, such as paraffins and olefins obtained from the Fischer-Tropsch synthesis.[23] The reverse water-gas shift (RWGS, eq. 1) reaction is an endothermic process that produces CO at relatively elevated temperatures (500–600 °C).[24] This reaction is sensitive to the C/H ratio on the catalyst surface. Due to the relative low heat of CO_2 adsorption, the fast hydrogenation of carbon intermediate species adsorbed on the surface is favoured. This leads to the formation of the unwanted methane by-product by the exothermic Sabatier reaction (eq. 2).[25]

$$CO_2 + H_2 \rightleftharpoons CO + H_2O \qquad \Delta H_{25\,^\circ C} = 41.2 \text{ kJ mol}^{-1} \quad (1)$$

$$CO_2 + 4\,H_2 \rightleftharpoons CH_4 + 2\,H_2O \qquad \Delta H_{25\,^\circ C} = -165 \text{ kJ mol}^{-1} \quad (2)$$

The main objectives when performing the RWGS are decreasing the reaction temperature while maintaining high conversion levels, and avoiding the production of undesired methane. Copper-based catalysts have been widely studied, with the main focus of elucidating the reaction mechanism.[26,27] Liu *et al.* reported that at temperatures below 600 °C in Cu-Ni/ɣ-Al_2O_3 systems, Cu favours the formation of CO while Ni favours CH_4 production.[28] Noble metal-based catalysts are very popular due to their high hydrogenation ability. However, they are expensive and tend to yield mainly methane. Promoters are used to improve the selectivity.[29] For example, among different mono- and bi-metallic noble metal catalysts, PtCo/ɣ-Al_2O_3 showed the highest selectivity to CO with little CH_4 production.[30] However, the high cost of noble metals makes them unattractive for large scale applications. Transition metal carbides (TMCs) are a promising type of catalysts that showed activity in RWGS. Porosoff *et al.* reported that the catalytic performance of molybdenum carbide (Mo_2C) catalyst was much better than those of bimetallic noble metal-based systems (PtCo, PtNi,

PdCo, PdNi supported on CeO_2).[31] Mo_2C catalyst gave 8.7% CO_2 conversion and 93.9% CO selectivity at 300 °C. Transition metal carbides are promising materials for RWGS due to their low cost and their potential to selectively perform at low temperatures.

Another possible product from CO_2 hydrogenation is methanol. Methanol is a very valuable precursor of products such as formaldehyde, dimethyl ether, gasoline and olefins.[32,33] It is also considered a potential fuel-substitute and an efficient energy storage chemical.[34–36] Production of methanol in industry uses mixed syngas ($CO/H_2/CO_2$) as feed and $Cu/ZnO/Al_2O_3$ as commercial catalyst. The reaction runs at 210–270 °C and 50–100 bar, and is highly selective towards methanol (99%).[37,38] The main drawback of this process is that methane steam reforming (SMR), a highly endothermic reaction that requires the combustion of natural gas, is used to produce the $CO_2/CO/H_2$ feedstock mix.[33] Efforts are being done to develop a direct methanol synthesis process independent of fossil fuels, using CO_2 combined with hydrogen produced from renewable energy.

Converting CO_2 to methanol (eq. 3) is an exothermic reaction, therefore favoured at lower temperatures.[39] It is also favoured at high pressures because fewer molecules are produced. Typically, the endothermic RWGS reaction (eq. 1) occurs in parallel, thus CO is produced as a side product, especially at higher temperatures. A compromise is usually reached at temperatures below 300 °C.

$$CO_2 + H_2 \rightleftharpoons CO + H_2O \qquad \Delta H_{25\,^\circ C} = 41.2 \text{ kJ mol}^{-1} \quad (1)$$

$$CO_2 + 3\,H_2 \rightleftharpoons CH_3OH + H_2O \qquad \Delta H_{25\,^\circ C} = -49.5 \text{ kJ mol}^{-1} \quad (3)$$

The catalyst design must take into account that, contrarily to the commercial methanol synthesis, CO_2 hydrogenation produces water as by-product, which can decrease catalyst activity and lifetime. The $Cu/ZnO/Al_2O_3$ catalyst used in the commercial production of methanol from $CO/H_2/CO_2$ was also tested in direct CO_2 hydrogenation to methanol. Optimization of the reaction parameters (H_2/CO_2 ratio of 10:1, 260 °C, 360 bar and 10,471 h^{-1} gas hourly space velocity, GHSV) over this catalyst achieved >95% of CO_2 conversion and >98% of methanol selectivity.[40] However, the pressure is too high for commercial application. Other Cu-based catalysts, especially Cu/ZnO catalysts, were widely studied.[27] Additives such as Al_2O_3, SiO_2 and Ga_2O_3 are added to enhance

activity, stability and thermal resistance. For example, a Cu-Zn-Ga layered catalyst was found to have a higher Cu surface area and dispersion, improving its catalytic performance compared to the commercial catalyst.[41] Pd-based catalysts were also studied despite its high cost. While Pd on its own is mainly selective to CO, the formation of the PdZn alloy enhances selectivity to methanol.[42] Supports such as TiO_2 and Al_2O_3 can be used to enhance the dispersion of the PdZn alloy.[43] Cheaper elements such as Ni or Co doped with Ga are promising materials, as seen in the volcano plot of Figure 1.4. Ni_5Ga_3 supported on SiO_2 yielded methanol at atmospheric pressure, in a temperature range of 150–250 °C and using a H_2/CO_2 ratio of 3:1.[44]

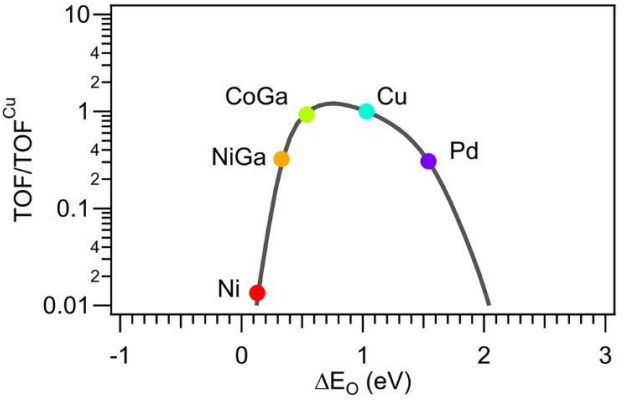

Figure 1.4. Volcano plot with the calculated turnover frequencies (TOF) relative to copper (TOF^{Cu}) of methanol synthesis as a function of oxygen binding energies (ΔE_O) for different active sites. Calculations were performed at 250 °C, 6.67 bar CO_2 and 23.33 bar H_2. Reproduced with permission from Springer Nature.[45]

Comparison with conventional $Cu/ZnO/Al_2O_3$ catalysts showed the same or better methanol synthesis activity, as well as considerably lower production of CO. In another study, Co_5Ga_3/SiO_2 catalyst showed promising selectivity towards methanol at 250 °C and 30 bar, although the conversion was lower than the commercial $Cu/ZnO/Al_2O_3$ catalyst.[45] Both NiGa and CoGa catalysts are promising materials for methanol production at relatively low pressures. However, gallium and its precursors are expensive, making these catalysts too costly (6 to 8 €/$g_{catalyst}$) compared to the commercial copper based catalyst (0.15 €/$g_{catalyst}$). Overall, CO_2 hydrogenation is usually performed at around 250 °C and

20 bar. Optimization of the catalyst composition and/or reaction conditions are needed to increase the competitiveness against the commercial process.

1.2. CO_2 and *n*-butane

Light alkanes (methane, ethane, propane and butane) can be used as feedstock in the chemical industry. Light alkanes, and specifically butane, can be found as side products in naphtha and oil cracking. Even if these side products are minor, they are valuable due to the vast amounts of fossil fuels that are currently consumed (11.7 billion toe in 2015).[5] Light alkanes are also present in shale gas. Although the main component of shale gas is methane (its concentration ranges from 50% to 90% of the total mixture), it also contains impurities such as nitrogen, carbon dioxide and longer light alkanes. The specific composition usually depends on the location of the shale gas source. The mixture of ethane, propane, *n*-butane, *i*-butane and pentane (also known as natural gas liquids, NGLs) can represent up to 50% of the shale gas composition, and butanes usually represent around 4% of the mixture.[46] The large volumes of cracking streams and shale gas, as well as their greenhouse effect when emitted to the atmosphere, make the production of high-added-value chemicals from light alkanes interesting.

Combination of light alkanes and CO_2 can result in the formation of syngas through dry reforming reactions (eq. 4).[47] Syngas is a common precursor of valuable chemicals, such as fuels or alcohols through the Fischer-Tropsch synthesis (FTS).[47,48] Dry reforming of methane (DRM, eq. 5) is the most studied dry reforming reaction, mostly because methane is widely available in shale gas, natural gas and biogas, and it is also considered a greenhouse gas when emitted to the atmosphere.[49] In addition, DRM gives a CO/H_2 ratio close to one, which makes it suitable for the production of long chain hydrocarbons through FTS. However, DRM is strongly endothermic, meaning that high temperatures (700–900 °C) are needed to achieve the desirable conversion levels. This results into fast catalyst deactivation by sintering (agglomeration of nanoparticles) and coking (deposition of carbon species on the active sites). Most studies focused on the development of non-noble metal catalysts due to their low cost, availability and high catalytic activity.[50,51] Ni-based catalysts are the most active catalysts, but they suffer severe deactivation problems due to sintering and

coking.[52] Different strategies have been studied to improve the stability of Ni-based catalysts, including the use of supports, promoters and second metals.[50–53] Despite its potential, the commercialization of DRM is limited by high temperature requirements and the low stability of the catalysts.

$$n\ CO_2 + C_nH_{2(n+1)} \rightleftharpoons 2n\ CO + (n+1)\ H_2 \quad (4)$$

$$CO_2 + CH_4 \rightleftharpoons CO + H_2 \qquad \Delta H_{25\ ^\circ C} = 247.3\ kJ\ mol^{-1} \quad (5)$$

$$4\ CO_2 + C_4H_{10} \rightleftharpoons 8\ CO + 5\ H_2 \quad \Delta H_{25\ ^\circ C} = 817.1\ kJ\ mol^{-1} \quad (6)$$

N-butane is thermodynamically less stable ($\Delta G^0_{(n\text{-}C4H10)}$ = -16.57 kJ/mol) than methane ($\Delta G^0_{(CH4)}$ = -50.45 kJ/mol), making dry reforming of butane (DRB, eq. 6) an interesting alternative to DRM. DRB can operate at lower temperatures (500–600 °C),[54] decreasing catalyst deactivation by sintering. However, coking remains an issue in DRB, due to the large number of coke sources. Formation of coke during dry reforming can come from the deposition of carbon atoms and/or from the formation of olefins. Carbon atoms are typically formed by the Boudouard reaction (2CO → CO_2 + C), but they can also be a product of the total cracking of butane.[55–57] Partial cracking or dehydrogenation of butane produces olefins, which can condensate and form polycyclic aromatic compounds.[58]

Although few studies focused on DRB (Table 1.2), a common factor is the use of Ni-based catalysts. Panczyk *et al.* studied the effect of doping a commercial Ni/Al_2O_3 catalyst with Mo, W, Ba, K and Ce.[59] The addition of promoters increased resistance towards coking, although all the catalysts experienced strong coking after 20 min under stream. Yan *et al.* studied the reaction using a bimetallic PtNi/CeO_2 catalyst, with a Pt/Ni ratio of 1:3.[60] The catalyst showed 20% CO_2 conversion and 15% butane conversion at 600 °C and CO_2 to butane ratio of 4:1. Although the PtNi catalyst showed slight deactivation, the conversion values and its resistance to coking were enhanced compared to the monometallic analogues, showing the benefits of the PtNi alloy. Li *et al.* studied the behaviour of a 1.5 wt.% Ni - 0.5 wt.% Fe/CeO_2 catalyst at 600 °C, using a CO_2 to butane ratio of 2:1.[61] After an initial decrease in activity due to coking, the catalyst showed 59.3% CO_2 conversion and 30.9% butane conversion after 8-10 hours at steady state. However, in this case the bimetallic catalyst did not show a significant improvement in the catalytic behaviour compared to the monometallic Ni/CeO_2 catalyst. Overall, DRB commercialization is interesting

due to its reduced energy cost compared to DRM. However, more research on catalyst development needs to be done to inhibit coking, and therefore increase catalyst lifetime.

Table 1.2. CO_2 conversion (X_{CO_2}), butane conversion (X_{Bu}), turnover frequency values (TOF) and CO selectivity (S_{CO}) monometallic and bimetallic catalysts during dry reforming of butane (at 600 °C and 1 atm).

Catalyst	X_{CO_2} (%)	X_{Bu} (%)	TOF_{CO_2} [a]	TOF_{Bu} [a]	S_{CO} (%)	CO_2/Bu ratio	Ref
Pt/CeO_2	1	1	31	12	56	4:1	61
Ni/CeO_2	12	9	628	112	98	4:1	61
Pt_1Ni_3/CeO_2	19	12	552	92	98	4:1	61
Ni/CeO_2	64	31	6852	1662	96	2:1	62
Fe/CeO_2	11	7	876	292	54	2:1	62
Ni_3Fe_1/CeO_2	59	31	3506	914	91	2:1	62

[a]TOF units: $mol \cdot mol_{metal}^{-1} \cdot min^{-1}$

Lower olefins ($C_2^=$–$C_4^=$) can be another product of light alkanes. Lower olefins are important chemicals for the production of plastics, synthetic textiles, rubbers, solvents and coatings.[23] These olefins are traditionally obtained from the cracking of naphtha in the oil refining industry. They are also obtained on large-scale from the dehydrogenation of alkanes (eq. 7). Several companies, such as Linde-BASF and Clariant (with the CATOFIN catalyst, Figure 1.5), commercially produce propene and butenes using chromium-alumina dehydrogenation catalysts.[62] Yet, these processes require high temperatures (>550 °C) because of the endothermic nature of the reaction.[63] As a side-reaction, thermal cracking generates coke on the catalyst surface, leading to the progressive deactivation of the catalyst and requiring periodic regeneration.

Oxidative dehydrogenation (ODH, eq. 8) of alkanes is an excellent alternative for the production of olefins. ODH is an exothermic reaction that can produce olefins at lower temperatures than direct dehydrogenation. The lower reaction temperature, and the possible removal of coke and its precursors by oxygen (air), increases catalyst stability. However, controlling the selectivity of this reaction is a huge challenge. Especially at high alkane conversion levels, selectivity to alkenes is restricted due to total oxidation to CO and CO_2. The use of oxygen also raises safety concerns, as the exothermic reaction forms

potentially flammable mixtures.[65] Alternating alkane and O_2 streams over a solid oxygen carrier (SOC) catalyst is a way to increase the safety of the process.[66,67]

Figure 1.5. Propane and butane dehydrogenation plant of Hengli Petrochemical (Dalian, China) Refinery Co., Ltd using the CATOFIN catalyst.[64]

$$C_nH_{2(n+1)} \rightleftharpoons C_nH_{2n} + H_2 \quad (7)$$

$$C_nH_{2(n+1)} + 0.5\ O_2 \rightleftharpoons C_nH_{2n} + H_2O \quad (8)$$

$$C_nH_{2(n+1)} + CO_2 \rightleftharpoons C_nH_{2n} + CO + H_2O \quad (9)$$

As an alternative to oxygen, CO_2 is emerging as a potentially greener oxidising agent. CO_2 has a lower oxidation strength than O_2, decreasing total oxidation and improving the selectivity to olefins. The safety of the process also increases by reducing the explosion risk. The disadvantage of using CO_2 is its high thermodynamic stability and the endothermic nature of CO_2-ODH. Therefore, CO_2-ODH usually requires higher reaction temperatures to obtain similar conversions than conventional O_2-ODH. In addition, oxidative dehydrogenation using CO_2 (CO_2-ODH, eq. 9) has the added value of using a greenhouse gas as feedstock to produce valuable chemicals. Considering the overall demand of C_2, C_3, and C_4 olefins ($8 \cdot 10^{12}$ mol/year),[68] and assuming that one mole of alkane reacts with one mole of CO_2, 0.34 Gt of CO_2 emissions could be avoided through CO_2-ODH. This represents 8.7% of the heavy industry emissions (see Table 1.1).

Of all lower alkanes, *n*-butane is a low cost and abundant raw material found in natural gas and as side product in naphtha and oil cracking. In addition, butenes and 1,3-butadiene (Figure 1.6) are important intermediates in synthetic chemistry. 1,3-butadiene is the key monomer for producing styrene butadiene

rubber (SBR), which is the main component of car tires. Other butenes are used mainly in the fuel industry. Isobutylene is a raw material for the synthesis of methyl tert-butyl ether (MTBE) and ethyl tert-butyl ether (ETBE), which are used as octane enhancers in gasoline.[23]

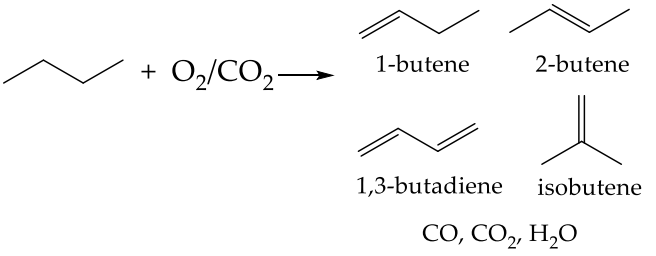

Figure 1.6. Possible products from butane oxidative dehydrogenation, using O_2 or CO_2 as oxidising agents.

Many studies on butane O_2-ODH focused on the application of transition metal oxides catalysts, specifically vanadium and molybdenum catalysts.[63,69–73] Vanadium oxide supported on MgO, denoted as VMgO, is one of the most studied catalysts.[63,74] The coexistence of MgO and orthovanadate ($Mg_3V_2O_8$) gave a good selectivity to butenes, while pyrovanadate ($Mg_2V_2O_7$) favored non-selective reactions.[75] Tellez *et al.* reported the performance of a VMgO catalyst with 24 wt.% of metallic vanadium.[76] At 500 °C and an oxygen to butane ratio of 2:1, the catalyst showed 78% selectivity to butenes at 5% butane conversion. More recently, the performance of vanadium dispersed on mesoporous titanosilicates catalysts has been explored (see table 1.3).[77,78] These catalysts are characterized by highly dispersed vanadium oxide species over the mesoporous structure given by the SiO_2, and excellent redox properties given by the titania and vanadia oxygen vacancies. These catalysts use a significant lower metal loading (1 wt.% V) than VMgO catalysts, and they are active at a lower temperature (460 °C). At this temperature, a V/Ti-SBA-15 catalyst showed its maximum selectivity to butene and butadiene (60%) at 6.1% butane conversion.[77]

Table 1.3. Performance of vanadia-based catalysts tested in butane ODH. X_{Bu} and S_{C_4} refer to butane conversion and butenes selectivity (monobutenes and 1,3-butadiene), respectively.

Catalyst	O_2:Butane ratio	Temperature (°C)	X_{Bu} (%)	S_{C_4} (%)	Ref
VMgO	2:1	520	5	75	76
VMgO	2:1	500	5	78	77
V/Ti-SBA-15	2:1	460	6	60	78
V/Ti-SBA-15	2:1	460	23	32	78
V/Ti-HMS	2:1	460	14	37	79

Work on vanadia-based catalysts remarks the importance of the oxygen vacancies or lattice oxygen species in the activation of *n*-butane.[77] Reducible metal oxide catalysts are believed to follow a Mars-van Krevelen (redox) mechanism, depicted in Figure 1.7. In this mechanism, the lattice oxygen atoms of the catalyst participate in the abstraction of hydrogen atoms from the alkane, producing the respective olefin and water. This results into reduced centres in the form of oxygen vacancies in the oxide lattice, which can react with O_2 to re-form the oxidized centres.[79,80]

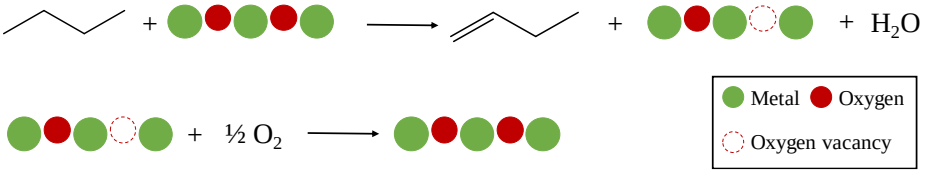

Figure 1.7. Oxidative dehydrogenation of *n*-butane to 1-butene, following the Mars-van Krevelen mechanism.

There are fewer published studies on butane CO_2-ODH.[68,81] Active catalysts in O_2-ODH are not always active in CO_2-ODH, as seen by previous studies using a VMgO catalyst (Table 1.4).[82] The effect of the support on vanadia-based catalysts was studied several times.[83] The good dispersion of vanadium oxide over a CeO_2-ZrO_2 support, combined with good redox properties, improved the catalytic performance compared to other supports (TiO_2-ZrO_2, SnO_2-ZrO_2 and ZrO_2).[84,85] 12 wt.% V_2O_5/CeO_2-ZrO_2 catalyst showed 40% butane conversion and 50% C_4 alkenes selectivity. However, CO_2-ODH conditions lead to faster catalyst

deactivation and parallel dry reforming of butane.[85] Li *et al.* performed CO_2-ODH at 600 °C and CO_2/butane ratio of 2:1.[61] In this study, a 0.5 wt.% Ni - 1.5 wt.% Fe/CeO_2-ZrO_2 catalyst showed the best dehydrogenation ability, showing 13.9% of butane conversion and 37.2% selectivity to C_4 alkenes. A catalyst with higher loading of nickel, 1.5 wt.% Ni - 0.5 wt.% Fe, mainly catalysed dry reforming of butane. Dasireddy *et al.* directly compared O_2 and CO_2 as oxidising agents over a Ni-Mo/Al_2O_3 catalyst.[86] At 450 °C, CO_2-ODH showed significant lower conversion but slightly higher selectivity compared to O_2-ODH (Table 1.4). Authors concluded that CO_2 increases alkenes selectivity by limiting the formation of electrophilic oxygen species (peroxide O_2^{2-} and superoxide O_2^-), which are believed to be responsible of the total oxidation of alkenes to CO_x species.[87] Overall, catalysts used in CO_2-ODH give lower activity than in O_2-ODH. This is likely related to the poor ability of CO_2 to re-oxidise the catalyst surface, and its tendency to stay adsorbed on the catalyst surface.[68] Bifunctional catalysts, which are able to effectively dissociate CO_2 and perform alkane dehydrogenation, need to be developed to increase CO_2-ODH conversion values while maintaining good alkene selectivity.

Table 1.4. Summary of catalysts tested in CO_2-ODH of butane.

Catalyst	Ox agent	Ox:Bu ratio	Temp. (°C)	X_{Bu} (%)	S_{C_4}(%)	Ref
VMgO	O_2	2:1	527	30	60	83
VMgO	CO_2	7.5:1	527	0	-	83
V_2O_5/SnO_2-ZrO_2	CO_2	5:1	600	20	35	85
V_2O_5/CeO_2-ZrO_2	CO_2	5:1	600	35	50	86
V_2O_5/TiO_2-ZrO_2	CO_2	5:1	600	40	25	86
Ni-Mo/Al_2O_3	O_2	2:1	450	71	57	87
Ni-Mo/Al_2O_3	CO_2	2:1	450	8	66	87

1.3. Exploring new catalyst families: MAX phases and MXenes

Supported catalysts, formed by metal or metal oxide nanoparticles dispersed over a supporting matrix, are commonly used in heterogeneous catalysis. Typically, the active component is the metal or metal oxide cluster, while the support is stable and unreactive. Commonly used supports are gamma alumina (ɣ-Al_2O_3), silica (SiO_2) and titania (TiO_2).[55] Although most of the attention is usually focused on the active site, the support plays a crucial role in catalysis. The support can indirectly enhance the reaction performance by increasing the dispersion of active sites and charge transfer effects, as well as modifying interface sites and nanoparticles morphology.[88] Most importantly, the support can prevent catalyst deactivation and boost the industrial application of high temperature reactions.[89]

For these reasons, we studied a new group of materials, namely **MAX phases**, as catalyst supports. MAX phases ($M_{n+1}AX_n$) are a family of layered ternary carbides and nitrides with hexagonal crystal structures.[90] Their name reflects their chemical composition, as represented in Figure 1.8. Typically, M is an early transition metal, A is an A-group element (mostly from groups 13 and 14), X is carbon or nitrogen, and n = 1, 2, or 3.[91] Since the 1960s, approximately 155 different MAX phases have been prepared.[92] MAX phases naturally classify by their n number into 211 (Ti_2AlC), 312 (Ti_3AlC_2) and 413 (Ti_4AlN_3) compounds, sharing a common structure consisting on $M_{n+1}X_n$ layers intercalated with pure A-group element layers (Figure 1.9).[91,93] The strong M-X bond has a mixed covalent, metallic and ionic character, whereas the M-A bond, with metallic character, is relatively weak.[93,94]

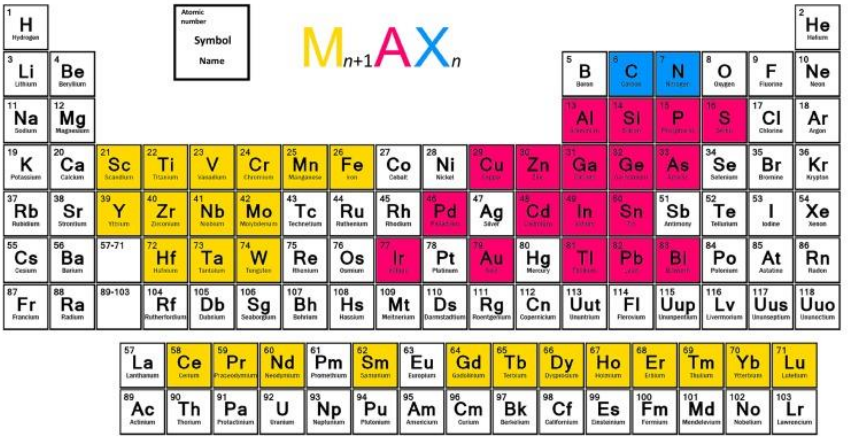

Figure 1.8. The MAX phase periodic table, with all elements incorporated in MAX phases up to date. Reproduced with permission from Elsevier.[92]

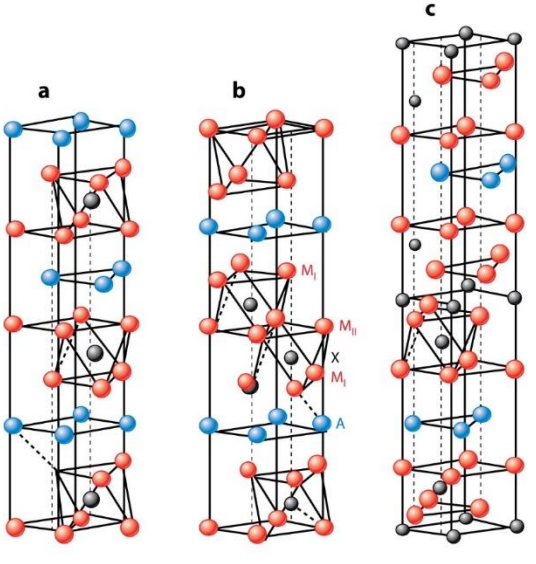

Figure 1.9. MAX phase unit cells: (a) 211, (b) 312, and (c) 413 phases. Every third layer in the 211 compounds (a) is an A-group, in the 312 (b), every fourth layer is an A-group, and in the 413 compounds (c), every fifth layer is an A-group. Reproduced from Annu. Rev. Mater. Res.[93]

MAX phases are interesting materials due to their unusual combination of properties. Like ceramics, they show high-temperature strength and stiffness, and at the same time they are tough, ductile, and conduct electricity and heat like metals.[95–97] In addition, they are easy to prepare at high temperature and pressures using solid solutions of the M, A or MX elements.[90] Due to these unique properties, MAX phases have been mainly used for mechanical and thermal applications,[98,99] such as structural coatings in fission and fusion reactors.[100,101] Only recently, Ng *et al.* showed that MAX phases also have interesting catalytic properties.[102] Though a carbide, Ti_3AlC_2 MAX phase catalysed butane oxidative dehydrogenation (ODH) with a higher selectivity than common oxide materials. The non-stoichiometric oxide surface layer containing oxygen vacancies made this material catalytically active.

In this thesis, we focus on Ti-based MAX phases, Ti_3AlC_2 and Ti_2AlC, as catalyst supports for high temperature reactions (500–700 °C). We were triggered by their high oxidation resistance, up to 1100 °C in the case of Ti_2AlC, which originates from the formation of an oxide protective layer.[95] In addition, their electronically rich surface and high conductivity might enhance the metal-support interactions compared to traditional supports, affecting the binding energy and reactivity of adsorbates. MAX phases also contain structural defects (dislocations) that can improve their reactivity.[91,102] They also have a good mechanical stability, which makes them resistant to manufacturing processes when scaling-up the reaction. MAX phases have a very low surface area (<10 m^2/g), which *a priori* might seem a disadvantage in catalysis.[103] Nevertheless, we were interested on studying the effect of this unusual combination of properties on the catalytic activity.

The selective etching of the A element from the MAX phases results in the formation of **MXenes**, a new family of two-dimensional (2D) transition metal carbides, nitrides and carbonitrides.[104] Since the synthesis of the first MXene ($Ti_3C_2T_x$) in 2011,[105] almost 30 new MXenes have been successfully prepared.[106] The interest on the application of MXenes arises from the enhanced interlayer space and surface area compared to MAX phases, as a result of the etching of the A element (Figure 1.10).[107,108] In addition, MXenes are hydrophilic, chemically stable and excellent electrical conductors.[104,109]

The general formula of MXenes is $M_{n+1}X_nT_x$, where M is an early transition metal, X is carbon and/or nitrogen, and n = 1, 2, or 3. T_x represents surface terminations such as fluorine, hydroxyl and/or oxygen atoms, depending on the etching method.[110] MXenes are typically prepared using aqueous fluoride-containing acidic solutions, such as hydrofluoric acid (HF) or a solution of hydrochloric acid (HCl) and lithium fluoride (LiF).[111] Other methods avoiding strong acids have been also developed, as summarized in reviews on the topic.[106,111,112] After etching, the selectively dissolved atomic layers are replaced by various terminations (T_x), and the multiple layers held together by weak interactions (hydrogen and/or van der Waals bonds).[106]

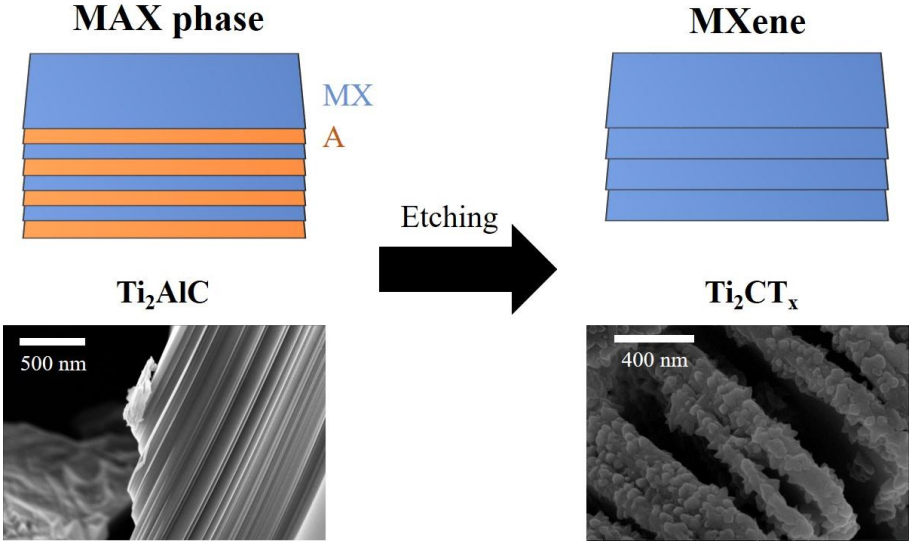

Figure 1.10. Schematic representation of the etching of a MAX phase to a MXene. SEM images show the tightly packed layers of Ti_2AlC MAX phase, compared to the Ti_2CT_x MXene.

The preparation method and post-synthesis treatments can tune the properties of the final MXene by changing the type of T_x surface terminations, the layer thickness and their thermal stability.[110] Due to their high electrical conductivity and the high ion diffusion rate between layers, MXenes have been mainly used for energy storage devices (such as Li-ion batteries and super-capacitors) and electrocatalysis.[106,108,113–115] The presence of functional surface groups and the

tunability of band gap structures in MXenes also boosted their application in photocatalysis.[104,116,117]

The potential of MXenes in heteregenous catalysts has been scarcely explored, even though they have a relatively high surface area and stability. Diao *et al.* found that $Ti_3C_2T_x$ MXene is active in the direct dehydrogenation of ethylbenzene.[118] Compared to graphene and nanodiamond, $Ti_3C_2T_x$ showed better conversion and selectivity. Li *et al.* tested a Nb_2CT_x MXene as support for platinum particles.[119] Water-gas shift reaction kinetics revealed that the reactive metal-support interactions (RMSI) stabilize the nanoparticles and creates alloy-MXene interfaces, which have a higher H_2O activation ability compared to a non-reducible or a bulk niobium carbide. We must continue exploring the potential of MXenes in thermal heterogeneous catalysis, so we can identify the active sites and elucidate the catalytic mechanisms of MXene-based catalysts.

1.4. Plasma-catalysis: An alternative to high temperature reactions

In the previous sections, we discussed some strategies to decrease reaction temperature in thermal-catalysis. The combination of CO_2 with high energy co-reactants, as well as the appropriate catalyst, can lower the energy penalty and the activation barrier of CO_2 conversion reactions. Despite these efforts, reaction temperatures in thermal-catalysis remain relatively high. For instance, CO_2 hydrogenation is usually performed at 250 °C or higher, while dry reforming reactions operate at 600–800 °C.

Activation of stable molecules like CO_2 by plasma-catalysis has a great potential because, contrarily to thermal activation, plasma activates directly the vibrational mode of the molecule. The energy is not wasted on the activation of other degrees of freedom that don't induce dissociation, such as rotational and translational modes. The energetic electrons in the plasma can activate inert molecules, while the bulk gas phase of the plasma remains near room temperature. Therefore, **using plasma-catalysis we can convert CO_2 to useful chemicals at near-ambient temperature and pressure.**

Plasma, also known as the 'fourth state of matter', is a partially ionized gas that contains electrons, excited molecules and atoms, radicals, ions and neutral gas species (Figure 1.11).[120] This ionized gas is usually created by

applying an electric discharge between two parallel electrodes, which are located inside a reactor filled with gas.[120]

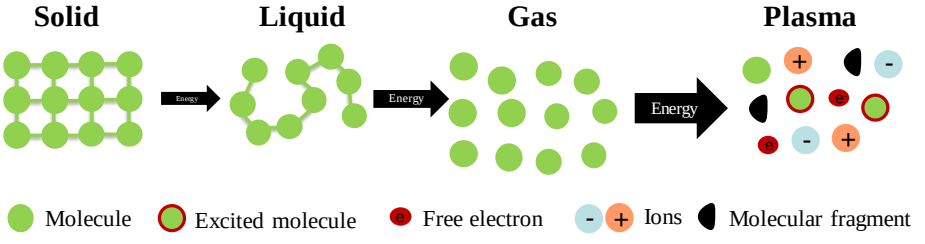

Figure 1.11. The four states of matter, ordered by increasing added energy.

There are two main types of plasma: high-temperature plasma (for example thermonuclear fusion plasmas) and low-temperature plasma. Low-temperature plasmas can be further classified into thermal and non-thermal plasmas, depending on the extent to which the species in the plasma reached thermal equilibrium. In thermal plasma, the applied energy and time for equilibration are sufficient for the species to reach the same temperature. Therefore, thermal plasma is defined by a single temperature. Plasma species in non-thermal plasmas do not have the same temperature, thus the plasma is characterised by multiple temperatures.

In non-thermal plasma, the bulk gas temperature (*i.e.*, the translational temperature of the heavy particles) remains low (300–1000 K), while the temperature of the electrons can be near 10^4–10^5 K. This is related to the higher kinetic energy of the electrons compared to the energy corresponding to the random motion of the molecules in the gas.[121] Therefore, non-thermal plasmas are far from the thermodynamic equilibrium. These hot electrons are responsible for the activation of stable gas molecules to reactive species such as radicals, excited atoms, molecules and ions. Fast moving electrons collide with heavier molecules, transfer their energy and cause reactions.[29]

There are two available ways for the energy transfer from the electron to the molecule. Firstly, in the single direct excitation all the required energy is transferred in one step. However, as the energy barrier is high for many reactions, only a few electrons can supply all the required energy to the molecule. The alternative way is the stepwise vibrational excitation, also known as vibrational ladder climbing, where the molecules reach the activation energy

through stepwise rise in energy (Figure 1.12). Several electron-molecule collisions induce molecule vibration. When the vibration is strong enough, the collision leads to dissociation or formation of radicals, which can react with other molecules and form new compounds. Compared to single direct excitation, the stepwise vibrational excitation requires less energy. In addition, a broader range of electrons with different energies can contribute to the activation through this way.[122]

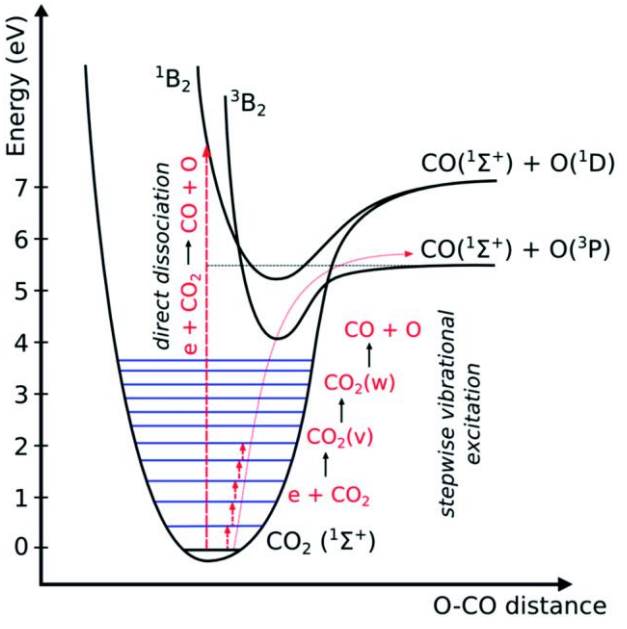

Figure 1.12. CO_2 electronic and vibrational levels during single direct excitation and stepwise vibrational excitation (ladder climbing). Reproduced from the Royal Society of Chemistry.[122]

Plasma alone is non-selective. The reactive species created by the electrons can recombine into many different products, and these products can be destroyed by new electron collisions. This was observed in a study on plasma assisted dry reforming of methane, where besides syngas, a significant amount of higher hydrocarbons (C_2-C_4), liquid hydrocarbons, polymers and oxygenates were also formed.[123] Therefore, in plasma-catalysis, the role of the catalyst is to regulate the selectivity towards a specific product, as well as lowering the activation energy barrier of the reaction.

Plasmas and catalysts can be combined in two main configurations, represented in Figure 1.13. In the two-stage configuration, the catalyst is placed separately from the plasma chamber, typically downstream of the plasma discharge. The typical lifetimes of vibrationally excited species at atmospheric pressure are extremely short (1–100 ns).[124] Therefore in a two-stage configuration these vibrational species are not involved in the reaction. Only the end-products and the long-lived intermediates interact with the catalyst.[120] In the single-stage configuration, the catalyst is directly placed in the discharge chamber. Besides long-lived species, the catalyst also interacts with the short-lived species of the plasma, including excited species, radicals, photons and electrons. In this configuration, the catalyst and the plasma influence each other. This might enhance the catalytic performance of a reaction compared to only plasma by increasing the reactants conversion and/or increasing selectivity to a certain product.

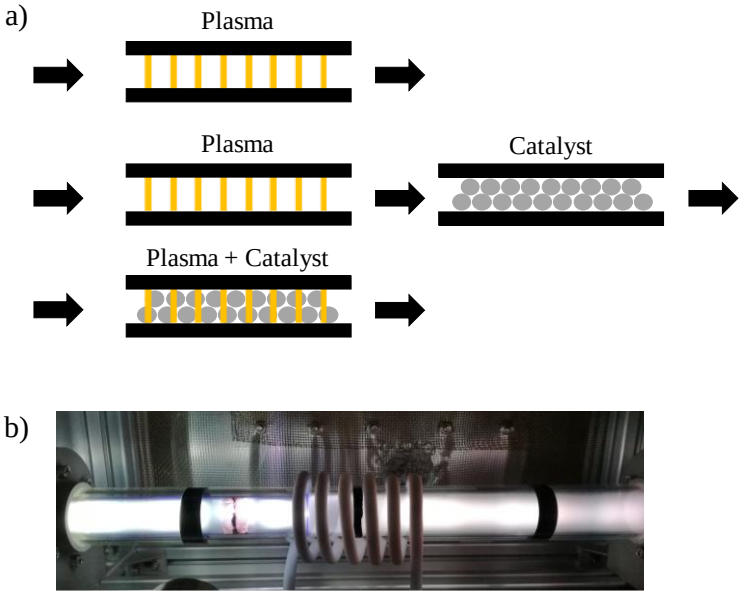

Figure 1.13. a) Scheme of different plasma-catalyst configurations. Only plasma without a catalyst (top), catalyst downstream of the plasma discharge (middle), and catalyst inside the discharge zone (bottom).[120] b) Catalyst inside a radio-frequency plasma discharge (white) during CO_2 hydrogenation.

There are several different types of non-thermal plasma depending on the electric field used to drive the plasma formation: microwave discharges, radio-

frequency discharges, glow discharges, gliding arc discharges and dielectric barrier discharges (DBDs), among others. Excellent reviews on plasma-catalysis describe in detail the operating conditions, configuration and properties of each type of plasma.[120,125,126] DBD plasma is by far the most studied option in plasma-catalysis. DBDs usually work at ambient temperature and atmospheric pressure, while the electrons are heated up to 20,000–30,000 K.[120] The main advantages of DBD plasmas are their low cost, simple operation and simple integration of a catalyst.

DBDs contain two electrodes surrounding the discharge volume, containing at least one dielectric barrier, as shown in Figure 1.14. The dielectric barrier is a material with high relative permittivity such as quartz, glass and ceramics. Its function is to limit the amount of charge and keep an equal distribution of charge over the electrode surface.[127] The DBD is a non-uniform plasma discharge, which consists of many little discharge channels, known as micro-discharges or filaments. These micro-discharges cover the surface of the dielectric material and extend across the discharge gap. The dielectric barrier limits the flow of current, and therefore the micro-discharges are extinguished. Sinusoidal alternating currents (AC) are used to build up again a sufficient field in the discharge gap and create a continuous pulsed behaviour plasma. This results in the continuous formation of nanosecond micro-discharges.[120,128]

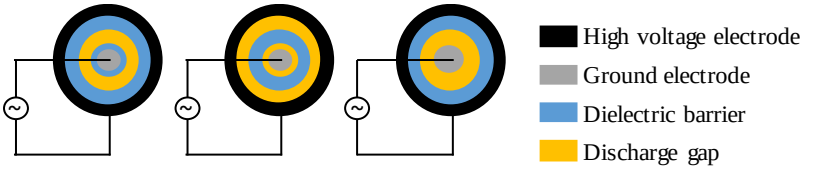

Figure 1.14. Basic configurations of the cylindrical dielectric barrier discharge.[120]

The combination of non-thermal plasma and a catalyst results in a complex chain of interactions. The chemical and physical properties of both the plasma and the catalyst can be modified by the presence of each other. These interactions often enhance the reaction in terms of conversion, selectivity and energy efficiency. The term 'synergy' is used when the combined effect of plasma and catalyst is larger than the sum of the two separate effects. However, it is very difficult to isolate the effects and directly relate to the catalytic activity. In order to clarify

the type of interactions in a plasma-catalyst system, they are divided into two categories: the effects of the catalyst on the plasma and the effects of the plasma on the catalyst.

The most common effects that the catalyst incurs on the plasma discharge are:

(1) Electric field enhancement. The electric field may be enhanced due to surface roughness and porosity of the catalyst.[129] This is attributed to polarization effects and the accumulation of charges on the surface of the packed material.[124] This effect is determined by the contact angle, the curvature and the dielectric constant of the packed material.[126] This physical effect leads to chemical effects on the plasma, since the electron impact dissociation and ionization rates are affected, influencing the chemical composition of the plasma and the energy efficiency of the reaction.[130]

(2) Formation of micro discharges inside the catalyst pores. Because the electric field inside the pores is very strong, the discharge characteristics between catalyst pores and plasma bulk are very different. This leads to different production and loss rates of the species in the plasma, and thus to a change in the plasma composition.[129] This enhanced field can lead to an increase on the concentration of active species.[130]

(3) Change in discharge type. The presence of a packing material promotes the development of different type of surface discharges, such as filamentary micro discharges and homogeneous surface discharges.[131] If the discharge can propagate along the catalyst surface, the plasma region can be expanded, creating more active species in the plasma volume and increasing the conversion of the reactants.[129,132] However, when the reactor is fully packed, the discharge mode can change from filamentary to predominantly surface discharges, which may decrease the conversion.[133,134]

(4) Reagent concentration in plasma. Gas molecules can be adsorbed on the catalyst surface, leading to an increase on the retention time and concentration in the plasma discharge zone. This could improve the conversion, selectivity and energy efficiency of the process, because of the higher probability of collisions between the adsorbed molecule and the active species generated in plasma.[130]

The plasma discharge can also affect the catalyst properties and how it interacts with the reactants. Some of the most commonly reported effects are:

(1) Change in the physicochemical properties of the catalyst. Plasma can induce several physicochemical changes on the catalyst surface. A number of effects have been experimentally observed, which are usually correlated to each other:

- The bombardment of the catalyst surface by plasma charged species can lead to the formation of smaller nanoparticles in the catalyst, increasing nanoparticles dispersion and total **surface area** of the catalyst.[133,135–137] In addition, compared to thermal-catalysis, temperatures in plasma-catalysis are lower, leading to less agglomeration of particles.
- Plasma can induce changes in the **oxidation state** of the catalyst. For example, a manganese catalyst in the form of Mn(III) was reduced to Mn(II,III) by active oxygen in the plasma.[137] The oxidation of Mn(IV) to Mn(V) by active oxygen was also reported.[138] Other species, such as adsorbed carbon coming from the fragmentation of CH_4 during dry reforming, were shown to reduce NiO to metallic Ni.[139]

(2) Formation of hot spots. Non-thermal plasmas operate near or slightly above room temperature. Regions where the temperature is locally higher can be formed due to strong microdischarges in the vicinity of sharp edges and corners of adjacent catalyst pellets or catalyst pores.[140] This thermal effect might increase the catalytic activity.[126]

(3) Decrease in the plasma species activation barriers. Vibrationally excited species, which are more reactive than their ground state counterparts, are present in the plasma discharge. The internal energies of these species can be too low to perform reactions in the plasma gas phase. Compared to plasma alone, the activation energies for reactions involving vibrational species can be lowered when adsorbed to a catalyst surface.[120]

As mentioned earlier, plasma-catalysis can activate CO_2 near room temperature, which attracted the attention of researchers over the last decade. Studies on CO_2 conversion using DBD plasmas mainly focused on CO_2 splitting, dry reforming of methane and CO_2 hydrogenation reactions.[29,120,141][142] Here, we focus on recent studies on CO_2 hydrogenation in DBD plasma.

Previous work on CO_2 hydrogenation shows that CO is usually the main product, and CH_4 the main side product.[143–147] For example, Liu *et al.* tested a series of perovskites using a H_2/CO_2 ratio of 1:1 in a DBD plasma at low temperature (35–120 °C) and atmospheric pressure.[145] At 90W, a La-Sr-Ni-Fe-O perovskite showed the best performance: 56% of CO_2 conversion and 84% selectivity to CO, almost suppressing the formation of CH_4. These values were superior to plasma only and to other perovskites (La-Ni-O, La-Sr-Ni-O and La-Sr-Fe-O). Its good catalytic performance was attributed to the formation of a uniform Ni-Fe alloy, a good metal-support interaction and to the enhanced redox properties of this catalyst. Sun *et al.* combined DBD plasma with a Pd/ZnO catalyst, which is commonly used in thermal-catalysis for the production of methanol.[146] At a H_2/CO_2 ratio of 3:1 and at a power of 30 W, the catalyst improved the reaction performance compared to only plasma, showing 32.5% of CO_2 conversion and 96.6% selectivity to CO. *In situ* spectroscopy indicated that the Pd-ZnO interface promotes the formation of carbonates and formates, which are reaction intermediates.

In addition to CO, small amounts of methanol and dimethyl ether were also detected in some studies.[148,149] Only recent studies reported a significant production of methanol by plasma-catalysis. For example, Wang *et al.* examined the effect of 15 wt.% Cu/γ-Al_2O_3 and 1 wt.% Pt/γ-Al_2O_3 catalysts on CO_2 hydrogenation, using a H_2/CO_2 ratio of 3:1 and a specially designed water-cooled DBD reactor.[150] Both catalysts increased CO_2 conversion and the concentration of methanol compared to only plasma. Cu/γ-Al_2O_3 catalyst enhanced the CO_2 conversion from 13% to 21.2%, and the methanol yield from 7.2% to 11.3%. The methanol selectivity was kept around 54%, but CO selectivity also increased from 30% to 40%. These changes in conversion and selectivity indicate the presence of plasma-assisted surface reactions in addition to the gas phase reactions when plasma and a catalyst are placed together. Men *et al.* also observed a significant production of methanol (23.2% methanol yield) by plasma-catalysis.[151] Highly dispersed Pt nanoparticles on a cold-plasma/peptide-assembly (CPPA) film and further combined with In_2O_3 were prepared and tested in the DBD plasma discharge at 30 W. The catalyst showed 37% of CO_2 conversion and 62.6% methanol selectivity. Authors relate the good performance of the Pt/film/In_2O_3 catalyst to the large surface area of the catalyst that leads to a high Pt dispersion and to a large metal-support interface, which

promotes CO_2 adsorption and conversion. In addition, CO_2 adsorption studies using FTIR show that the catalyst also produces methoxy species, which are key intermediate species in methanol production.

In general, plasma-catalysis has a positive effect on CO_2 conversion and selectivity to a specific product compared to only plasma. However, there is still little understanding on the fundamental reasons of this enhancement. Isolating the effects of combining plasma and a catalyst, and directly relating these to the catalytic activity, is difficult. We must continue studying the effect of introducing different packing materials in plasma reactors, so we can understand the relationship between catalyst properties and the reaction performance. *In-situ* spectroscopy techniques are also being developed to identify the reaction intermediates, and therefore reveal the possible reaction mechanisms in plasma-catalysis. Ultimately, we will be able to rationally design catalysts for plasma reactions, instead of basing our research on previous thermal-catalysis work.

1.5. Scope of this thesis

This thesis describes different ways of converting CO_2 to high value-added chemicals. For that, we tested traditional (γ-Al_2O_3, TiO_2 and MgO based catalysts) and non-traditional (MAX phase and MXene based catalysts) materials in different thermocatalytic reactions: butane dry reforming (where CO_2 reacts with butane to produce syngas), reverse water-gas shift (RWGS, where CO_2 reacts with H_2 to CO and H_2O), and butane oxidative dehydrogenation (ODH) to produce butenes. In addition to thermal-catalysis, we used plasma-catalysis to perform CO_2 splitting and CO_2 hydrogenation to methanol. The remainder of this thesis comprises five chapters.

Motivated by the unusual set of properties that MAX phases present and the little knowledge about their application in catalysis, in **Chapter 2** we report the studies of a Ti_2AlC-supported cobalt oxide catalyst in the dry reforming of butane reaction. We compared its properties and catalytic performance to traditional catalysts, Co_3O_4/TiO_2 and Co_3O_4/γ-Al_2O_3. We found that the thermal stability and basicity of Ti_2AlC increases the coke resistance, and therefore stability over time, of Co_3O_4/Ti_2AlC catalyst.

Chapter 3 examines the potential of Ti_3AlC_2 MAX phase as a support for molybdenum oxide for the reverse water-gas shift reaction (RWGS), comparing this new catalyst to more traditional materials. The catalyst showed higher intrinsic activity than MoO_3/TiO_2 and MoO_3/Al_2O_3 catalysts, due to the exceptional electronic properties of the Ti_3AlC_2 support that enhance the reducibility of MoO_3 species during reaction.

In **Chapter 4,** we describe the potential of a 2D Ti_2CT_x MXene in butane oxidative dehydrogenation (ODH). We found that the material was partially oxidised after synthesis, and completely oxidised after ODH. Nevertheless, the presence of vacancies and the electronic properties of the TiO_2/Ti_2CT_x material enhanced its conversion and selectivity during O_2-ODH. A commercial TiC catalyst showed lower conversion and selectivity than the MXene-derived catalyst. In addition, the TiO_2/Ti_2CT_x catalyst was not active when CO_2 was used as an oxidising agent.

In **Chapter 5,** we report the use plasma-catalysis to convert CO_2 near ambient conditions. We performed CO_2 hydrogenation in a DBD plasma reactor near room temperature and ambient pressure. We found that basic MgO support was more active than the acidic γ-Al_2O_3. MgO-supported cobalt oxide catalysts with a good metal-support dispersion improved the conversion and the methanol selectivity.

Finally, **Chapter 6** looks at the effects of plasma-catalysis during CO_2 splitting in a radio-frequency plasma setup. The combination of plasma and metal meshes enhanced CO_2 conversion compared to plasma alone. We believe that impact dissociation of excited CO_2 is favoured on surface defects (steps) of the metal meshes. After CO_2 dissociation to CO and O atoms, the metal meshes also act as recombination catalysts of oxygen atoms, avoiding the undesired recombination of CO and O atoms to CO_2. We also found that metal oxide catalysts have no effect on CO_2 conversion under these conditions, as they don't promote the impact dissociation mechanism.

1.6. References

[1] **High-resolution carbon dioxide concentration record 650,000-800,000 years before present**, D. Lüthi, M. Le Floch, B. Bereiter, T. Blunier, J.M. Barnola, U. Siegenthaler, D. Raynaud, J. Jouzel, H. Fischer, K. Kawamura, T.F. Stocker, *Nature* **2008**, *453*, 379–382.

[2] **Reduction of CO_2 to Chemicals and Fuels: A Solution to Global Warming and Energy Crisis**, S.C. Peter, *ACS Energy Lett.* **2018**, *3*, 1557–1561.

[3] **Shell Scenarios. Sky. Meeting the goals of The Paris agreement**, Shell International B.V., 'Shell Scenarios. Sky. Meeting the goals of The Paris agreement', can be found under www.shell.com/skyscenario, **2018**.

[4] **Shell Scenarios. The numbers behind Sky.**, Shell International B.V., 'Shell Scenarios. The numbers behind Sky.', can be found under www.shell.com/skyscenario, **2018**.

[5] **Chemical Technology. From Principles to Products.**, A. Jess, P. Wasserscheid, Wiley-VCH Verlag GmbH & Co. KGaA, **2020**, pp. 387–388.

[6] **Renewable energy in Europe – 2018: Recent growth and knock-on effects**, European Enviornmental Agency (EEA), 'Renewable energy in Europe – 2018: Recent growth and knock-on effects', can be found under https://www.eea.europa.eu/publications/renewable-energy-in-europe-2018, **2018**.

[7] **Renewable Energy Prospects for the European Union**, International Renewable Energy Agency (IRENA), 'Renewable Energy Prospects for the European Union', can be found under https://www.irena.org/-/media/Files/IRENA/Agency/Publication/2018/Feb/IRENA_REmap_EU_2018.pdf, **2018**.

[8] **Renewable energy market analysis: Southeast Asia**, International Renewable Energy Agency (IRENA), 'Renewable energy market analysis: Southeast Asia', can be found under https://www.irena.org/-/media/Files/IRENA/Agency/Publication/2018/Jan/IRENA_Market_Southeast_Asia_2018.pdf, **2018**.

[9] **Carbon capture, storage and utilisation technologies: A critical analysis and comparison of their life cycle environmental impacts**, R.M. Cuéllar-Franca, A. Azapagic, *J. CO_2 Util.* **2015**, *9*, 82–102.

[10] **Comparison of solvents for post-combustion capture of CO_2 by chemical absorption**, A. Kothandaraman, L. Nord, O. Bolland, H.J. Herzog, G.J. McRae, *Energy Procedia* **2009**, *1*, 1373–1380.

[11] **Generation, capture, and utilization of industrial carbon dioxide**, A.J. Hunt, E.H.K. Sin, R. Marriott, J.H. Clark, *ChemSusChem* **2010**, *3*, 306–322.

[12] **Transformation of carbon dioxide**, T. Sakakura, J.C. Choi, H. Yasuda, *Chem. Rev.* **2007**, *107*, 2365–2387.

[13] **Promoting the Synthesis of Methanol: Understanding the Requirements for an Industrial Catalyst for the Conversion of CO_2**, M. Behrens, *Angew. Chem. Int. Ed.* **2016**, *55*, 14906–14908.

[14] **Carbon Recycling International**, 'Carbon Recycling International', can be found under http://www.carbonrecycling.is/george-olah.

[15] **What Should We Make with CO_2 and How Can We Make It?**, O.S. Bushuyev, P. De Luna, C.T. Dinh, L. Tao, G. Saur, J. van de Lagemaat, S.O. Kelley, E.H. Sargent, *Joule* **2018**, *2*, 825–832.

[16] **Energy related CO_2 conversion and utilization: Advanced materials/nanomaterials, reaction mechanisms and technologies**, Y. Zheng, W. Zhang, Y. Li, J. Chen, B. Yu, J. Wang, L. Zhang, J. Zhang, *Nano Energy* **2017**, *40*, 512–539.

[17] **Non-thermal plasma technology for the conversion of CO_2**, B. Ashford, X. Tu, *Curr. Opin. Green Sustain. Chem.* **2017**, *3*, 45–49.

[18] **Plasma Assisted Catalytic Conversion of CO_2 and H_2O Over Ni/Al_2O_3 in a DBD Reactor**, X. Ma, S. Li, M. Ronda-Lloret, R. Chaudhary, L. Lin, G. van Rooij, F. Gallucci, G. Rothenberg, N.R. Shiju, V. Hessel, *Plasma Chem. Plasma Process.* **2019**, *39*, 109–124.

[19] **Tuning of conversion and optical emission by electron temperature in inductively coupled CO_2 Plasma**, D. Zhang, Q. Huang, E.J. Devid, E. Schuler, N.R. Shiju, G. Rothenberg, G. Van Rooij, R. Yang, K. Liu, A.W. Kleyn, *J. Phys. Chem. C* **2018**, *122*, 19338–19347.

[20] **Direct methane conversion routes to chemicals and fuels**, M.C. Alvarez-Galvan, N. Mota, M. Ojeda, S. Rojas, R.M. Navarro, J.L.G. Fierro, *Catal. Today* **2011**, *171*, 15–23.

[21] **CO_2 recycling: A key strategy to introduce green energy in the chemical production chain**, S. Perathoner, G. Centi, *ChemSusChem* **2014**, *7*, 1274–1282.

[22] **Can we afford to waste carbon dioxide? Carbon dioxide as a valuable source of carbon for the production of light olefins**, G. Centi, G. Iaquaniello, S. Perathoner, *ChemSusChem* **2011**, *4*, 1265–1273.

[23] **A Critical Look at Direct Catalytic Hydrogenation of Carbon Dioxide to Olefins**, M. Ronda-Lloret, G. Rothenberg, N.R. Shiju, *ChemSusChem* **2019**, *12*, 3896–3914.

[24] **Recent advances in catalytic hydrogenation of carbon dioxide**, W. Wang, S. Wang, X. Ma, J. Gong, *Chem. Soc. Rev.* **2011**, *40*, 3703–3727.

[25] **Directly converting CO_2 into a gasoline fuel**, J. Wei, Q. Ge, R. Yao, Z. Wen, C. Fang, L. Guo, H. Xu, J. Sun, *Nat. Commun.* **2017**, *8*, 15174.

[26] **Recent advances in catalytic hydrogenation of carbon dioxide**, W. Wang, S.P. Wang, X.B. Ma, J.L. Gong, *Chem. Soc. Rev.* **2011**, *40*, 3703–3727.

[27] **Catalytic reduction of CO_2 by H_2 for synthesis of CO, methanol and hydrocarbons: Challenges and opportunities**, M.D. Porosoff, B. Yan, J.G. Chen, *Energy Environ. Sci.* **2016**, *9*, 62–73.

[28] **Study of bimetallic Cu-Ni/γ-Al_2O_3 catalysts for carbon dioxide hydrogenation**, Y. Liu, D. Liu, *Int. J. Hydrog. Energy* **1999**, *24*, 351–354.

[29] **Hydrogenation of carbon dioxide to value-added chemicals by heterogeneous catalysis and plasma catalysis**, M. Liu, Y. Yi, L. Wang, H. Guo, A. Bogaerts, *Catalysts* **2019**, *9*, 275.

[30] **Trends in the catalytic reduction of CO_2 by hydrogen over supported monometallic and bimetallic catalysts**, M.D. Porosoff, J.G. Chen, *J. Catal.* **2013**, *301*, 30–37.

[31] **Molybdenum carbide as alternative catalysts to precious metals for highly selective reduction of CO_2 to CO**, M.D. Porosoff, X. Yang, J.A. Boscoboinik, J.G. Chen, *Angew. Chem. Int. Ed.* **2014**, *53*, 6705–6709.

[32] **Conversion of methanol to hydrocarbons: How zeolite cavity and pore size controls product selectivity**, U. Olsbye, S. Svelle, M. Bjrgen, P. Beato, T.V.W. Janssens, F. Joensen, S. Bordiga, K.P. Lillerud, *Angew. Chem. Int. Ed.* **2012**, *51*, 5810–5831.

[33] **Methanol Synthesis from CO_2 Hydrogenation**, M. Bowker, *ChemCatChem* **2019**, *11*, 4238–4246.

[34] **New Strategies for CO_2-to-Methanol Conversion**, J. Choudhury, *ChemCatChem* **2012**, *4*, 609–611.

[35] **Beyond oil and gas: The methanol economy**, G.A. Olah, *Angew. Chem. Int. Ed.* **2005**, *44*, 2636–2639.

[36] **Selective transformation of carbon dioxide into lower olefins with a bifunctional catalyst composed of $ZnGa_2O_4$ and SAPO-34**, X. Liu, M. Wang, C. Zhou, W. Zhou, K. Cheng, J. Kang, Q. Zhang, W. Deng, Y. Wang, *Chem. Commun.* **2017**, *54*, 140–143.

[37] **Design and simulation of a methanol production plant from CO_2 hydrogenation**, É.S. Van-Dal, C. Bouallou, *J. Clean. Prod.* **2013**, *57*, 38–45.

[38] **Comparison between two methods of methanol production fromcarbon dioxide**, B. Anicic, P. Trop, D. Goricanec, *Energy* **2014**, *77*, 279–289.

[39] **Highly Selective Conversion of Carbon Dioxide to Lower Olefins**, Z. Li, J.

Wang, Y. Qu, H. Liu, C. Tang, S. Miao, Z. Feng, H. An, C. Li, *ACS Catal.* **2017**, *7*, 8544–8548.

[40] **Towards full one-pass conversion of carbon dioxide to methanol and methanol-derived products**, A. Bansode, A. Urakawa, *J. Catal.* **2014**, *309*, 66–70.

[41] **CO_2 Hydrogenation to Methanol over Catalysts Derived from Single Cationic Layer CuZnGa LDH Precursors**, M.M.J. Li, C. Chen, T. Ayvall, H. Suo, J. Zheng, I.F. Teixeira, L. Ye, H. Zou, D. O'Hare, S.C.E. Tsang, *ACS Catal.* **2018**, *8*, 4390–4401.

[42] **Pd/ZnO catalysts for direct CO_2 hydrogenation to methanol**, H. Bahruji, M. Bowker, G. Hutchings, N. Dimitratos, P. Wells, E. Gibson, W. Jones, C. Brookes, D. Morgan, G. Lalev, *J. Catal.* **2016**, *343*, 133–146.

[43] **PdZn catalysts for CO_2 hydrogenation to methanol using chemical vapour impregnation (CVI)**, H. Bahruji, M. Bowker, W. Jones, J. Hayward, J. Ruiz Esquius, D.J. Morgan, G.J. Hutchings, *Faraday Discuss.* **2017**, *197*, 309–324.

[44] **Discovery of a Ni-Ga catalyst for carbon dioxide reduction to methanol**, F. Studt, I. Sharafutdinov, F. Abild-Pedersen, C.F. Elkjær, J.S. Hummelshøj, S. Dahl, I. Chorkendorff, J.K. Nørskov, *Nat. Chem.* **2014**, *6*, 320–324.

[45] **Theoretical and Experimental Studies of CoGa Catalysts for the Hydrogenation of CO_2 to Methanol**, J.A. Singh, A. Cao, J. Schumann, T. Wang, J.K. Nørskov, F. Abild-Pedersen, S.F. Bent, *Catal. Letters* **2018**, *148*, 3583–3591.

[46] **Valorization of shale gas condensate to liquid hydrocarbons through catalytic dehydrogenation and oligomerization**, T. Ridha, Y. Li, E. Gençer, J.J. Siirola, J.T. Miller, F.H. Ribeiro, R. Agrawal, *Processes* **2018**, *6*, 1–21.

[47] **Dry reforming of hydrocarbon feedstocks**, Y.T. Shah, T.H. Gardner, *Catal. Rev.* **2014**, *56*, 476–536.

[48] **Operating characteristics of transcritical CO_2 heat pump for simultaneous water cooling and heating**, J. Sarkar, S. Bhattacharyya, *Arch. Thermodyn.* **2012**, *33*, 23–40.

[49] **An overview on dry reforming of methane: Strategies to reduce carbonaceous deactivation of catalysts**, S. Arora, R. Prasad, *RSC Adv.* **2016**, *6*, 108668–108688.

[50] **Dry reforming of methane using various catalysts in the process: review**, R. Singh, A. Dhir, S.K. Mohapatra, S.K. Mahla, *Biomass Convers. Biorefinery* **2019**, DOI 10.1007/s13399-019-00417-1.

[51] **Catalyst design for dry reforming of methane: Analysis review**, N.A.K. Aramouni, J.G. Touma, B.A. Tarboush, J. Zeaiter, M.N. Ahmad, *Renew. Sustain. Energy Rev.* **2018**, *82*, 2570–2585.

[52] **Progress in Synthesis of Highly Active and Stable Nickel-Based Catalysts for**

Carbon Dioxide Reforming of Methane, S. Kawi, Y. Kathiraser, J. Ni, U. Oemar, Z. Li, E.T. Saw, *ChemSusChem* **2015**, *8*, 3556–3575.

[53] **Dry Reforming of Methane Over Cobalt Catalysts: A Literature Review of Catalyst Development**, A.W. Budiman, S.H. Song, T.S. Chang, C.H. Shin, M.J. Choi, *Catal. Surv. from Asia* **2012**, *16*, 183–197.

[54] **Thermodynamic study of hydrocarbon synthesis from carbon dioxide and hydrogen**, B. Yao, W. Ma, S. Gonzalez-Cortes, T. Xiao, P.P. Edwards, *Greenh. Gas Sci Technol.* **2017**, *7*, 942–957.

[55] **Catalytic Technology for Carbon Dioxide Reforming of Methane to Synthesis Gas**, M.-S. Fan, A.Z. Abdullah, S. Bhatia, *ChemCatChem* **2009**, *1*, 192–208.

[56] **Carbon Dioxide Reforming of Methane To Produce Synthesis Gas over Metal-Supported Catalysts: State of the Art**, S. Wang, G.Q. (Max) Lu, G.J. Millar, *Energy & Fuels* **1996**, *10*, 896–904.

[57] **Coke formation during CO_2 reforming of CH_4 over alumina-supported nickel catalysts**, A.S.A. Al Fatish, A.A. Ibrahim, A.H. Fakeeha, M.A. Soliman, M.R.H. Siddiqui, A.E. Abasaeed, *Appl. Catal. A Gen.* **2009**, *364*, 150–155.

[58] **Study of coke deposited on a VO_x-K_2O/γ-Al_2O_3 catalyst in the non-oxidative dehydrogenation of isobutane**, Y.P. Tian, X.M. Liu, M.J. Rood, Z.F. Yan, *Appl. Catal. A Gen.* **2017**, *545*, 1–9.

[59] **Nickel-promoted catalysts in the reforming of n-butane with CO_2 or H_2O**, M. Pańczyk, G. Giecko, W. Gac, S. Pasieczna, B. Stasińska, T. Borowiecki, *Adsorpt. Sci. Technol.* **2001**, *19*, 4–9.

[60] **Dry Reforming of Ethane and Butane with CO_2 over PtNi/CeO_2 Bimetallic Catalysts**, B. Yan, X. Yang, J. Wan, M. Myint, S. Kattel, *ACS Catal.* **2016**, *6*, 7283–7292.

[61] **Oxidative dehydrogenation and dry reforming of n-butane with CO_2 over NiFe bimetallic catalysts**, X. Li, B. Yan, S. Yao, S. Kattel, J.G. Chen, T. Wang, *Appl. Catal. B Environ.* **2018**, *231*, 213–223.

[62] **Light alkane dehydrogenation to light olefin technologies: A comprehensive review**, Z. Nawaz, *Rev. Chem. Eng.* **2015**, *31*, 413–436.

[63] **Catalytic oxidative dehydrogenation of n-butane**, L.M. Madeira, M.F. Portela, *Catal. Rev. - Sci. Eng.* **2002**, *44*, 247–286.

[64] **Successful startup of world's largest dehydrogenation plant using clariant's catofin® catalyst technology**, 'Successful startup of world's largest dehydrogenation plant using clariant's catofin® catalyst technology', can be found under https://www.clariant.com/es/Corporate/News/2019/08/Successful-startup-of-worldrsquos-largest-dehydrogenation-plant-using-Clariantrsquos-CATOFINreg-cata.

[65] **Oxidative Dehydrogenation of Light Alkanes**, J.S. Valente, R. Quintana-Solorzano, H. Armendariz-Herrera, *Catal. Rev.* **2018**, *31*, 8.

[66] **Solvent-free synthesis of rechargeable solid oxygen reservoirs for clean hydrogen oxidation**, G. Rothenberg, E.A. De Graaf, A. Bliek, *Angew. Chem. Int. Ed.* **2003**, *42*, 3366–3368.

[67] **Two-step catalytic oxidative dehydrogenation of propane: An alternative route to propene**, E.A. De Graaf, G. Zwanenburg, G. Rothenberg, A. Bliek, *Org. Process Res. Dev.* **2005**, *9*, 397–403.

[68] **Carbon dioxide reduction in tandem with light-alkane dehydrogenation**, E. Gomez, B. Yan, S. Kattel, J.G. Chen, *Nat. Rev. Chem.* **2019**, *3*, 638–649.

[69] **Progress in selective oxidative dehydrogenation of light alkanes to olefins promoted by boron nitride catalysts**, L. Shi, Y. Wang, B. Yan, W. Song, D. Shao, A.H. Lu, *Chem. Commun.* **2018**, *54*, 10936–10946.

[70] **Oxidative dehydrogenation of ethane and propane: How far from commercial implementation?**, F. Cavani, N. Ballarini, A. Cericola, *Catal. Today* **2007**, *127*, 113–131.

[71] **Heterogeneous partial (Amm)oxidation and oxidative dehydrogenation catalysis on mixed metal oxides**, J.C. Védrine, *Catalysts* **2016**, *6*, DOI 10.3390/catal6020022.

[72] **Activity of Molybdenum Oxide Catalyst Supported on Al2O3, TiO2, and SiO2 Matrix in the Oxidative Dehydrogenation of n-Butane**, M. Setnička, Z. Tišler, D. Kubička, R. Bulánek, *Top. Catal.* **2015**, *58*, 866–876.

[73] **Oxidative Dehydrogenation of n-Butane: Activity and Kinetics over VOx/Al2O3 Catalysts**, N. Madaan, R. Haufe, N.R. Shiju, G. Rothenberg, *Top. Catal.* **2014**, *57*, 1400–1406.

[74] **Oxidative dehydrogenation of: N -butane to butenes on Mo-doped VMgO catalysts**, X. Liu, L. Duan, W. Yang, X. Zhu, *RSC Adv.* **2017**, *7*, 34131–34137.

[75] **Oxidative dehydrogenation of C_4 hydrocarbons over VMgO catalyst - Kinetic investigations**, A.A. Lemonidou, *Appl. Catal. A Gen.* **2001**, *216*, 277–284.

[76] **Oxidative dehydrogenation of butane over VMgO catalysts**, C. Téllez, M. Abon, J.A. Dalmon, C. Mirodatos, J. Santamaría, *J. Catal.* **2000**, *195*, 113–124.

[77] **Vanadium oxide supported on titanosilicates for the oxidative dehydrogenation of n -butane**, C. Wang, J.G. Chen, T. Xing, Z.T. Liu, Z.W. Liu, J. Jiang, J. Lu, *Ind. Eng. Chem. Res.* **2015**, *54*, 3602–3610.

[78] **Hexagonal mesoporous titanosilicates as support for vanadium oxide - Promising catalysts for the oxidative dehydrogenation of n-butane**, M. Setnička, P. Čičmanec, R. Bulánek, A. Zukal, J. Pastva, *Catal. Today* **2013**, *204*, 132–

139.

[79] **Dioxygen activation routes in Mars-van Krevelen redox cycles catalyzed by metal oxides**, S. Kwon, P. Deshlahra, E. Iglesia, *J. Catal.* **2018**, *364*, 228–247.

[80] **Heterogeneous partial oxidation catalysis on metal oxides**, J.C. Védrine, I. Fechete, *Comptes Rendus Chim.* **2016**, *19*, 1203–1225.

[81] **Carbon dioxide utilization as a soft oxidant and promoter in catalysis**, M.B. Ansari, S.E. Park, *Energy Environ. Sci.* **2012**, *5*, 9419–9437.

[82] **Effect of carbon dioxide on the reaction performance of oxidative dehydrogenation of n-butane over V-Mg-O catalyst**, S. Ge, C. Liu, S. Zhang, Z. Li, *Chem. Eng. J.* **2003**, *94*, 121–126.

[83] **CO_2 as a soft oxidant for oxidative dehydrogenation reaction: An eco benign process for industry**, D. Mukherjee, S.E. Park, B.M. Reddy, *J. CO_2 Util.* **2016**, *16*, 301–312.

[84] **Synthesis of C4 olefins from n-butane over a novel VO_x/SnO_2-ZrO_2 catalyst using CO_2 as soft oxidant**, G. Raju, B.M. Reddy, B. Abhishek, Y.H. Mo, S.E. Park, *Appl. Catal. A Gen.* **2012**, *423–424*, 168–175.

[85] **CO_2 promoted oxidative dehydrogenation of n-butane over VO_x/MO_2-ZrO_2 (M = Ce or Ti) catalysts**, G. Raju, B.M. Reddy, S.E. Park, *J. CO_2 Util.* **2014**, *5*, 41–46.

[86] **Effect of O_2, CO_2 and N_2O on Ni-Mo/Al_2O_3 catalyst oxygen mobility in n-butane activation and conversion to 1,3-butadiene**, V.D.B.C. Dasireddy, M. Huš, B. Likozar, *Catal. Sci. Technol.* **2017**, *7*, 3291–3302.

[87] **Improving the alkene selectivity of nanocarbon-catalyzed oxidative dehydrogenation of n-butane by refinement of oxygen species**, J. Li, P. Yu, J. Xie, J. Liu, Z. Wang, C. Wu, J. Rong, H. Liu, D. Su, *ACS Catal.* **2017**, *7*, 7305–7311.

[88] **Control of metal-support interactions in heterogeneous catalysts to enhance activity and selectivity**, T.W. Deelen, C.H. Mejía, K.P. Jong, *Nat. Catal.* **2019**, *2*, 955–970.

[89] **Redox properties of doped and supported copper-ceria catalysts**, J. Beckers, G. Rothenberg, *Dalt. Trans.* **2008**, 6573–6578.

[90] **Progress in research and development on MAX phases: A family of layered ternary compounds**, Z.M. Sun, *Int. Mater. Rev.* **2011**, *56*, 143–166.

[91] **The MAX Phases: Unique New Carbide and Nitride Materials**, M. Barsoum, T. El-Raghy, *Am. Sci.* **2001**, *89*, 334–343.

[92] **On the Chemical Diversity of the MAX Phases**, M. Sokol, V. Natu, S. Kota, M.W. Barsoum, *Trends Chem.* **2019**, *1*, 210–223.

[93] **Elastic and Mechanical Properties of the MAX Phases**, M.W. Barsoum, M.

Radovic, *Annu. Rev. Mater. Res.* **2011**, *41*, 195–227.

[94] **Bonding and classification of nanolayered ternary carbides**, Z. Sun, D. Music, R. Ahuja, S. Li, J.M. Schneider, *Phys. Rev. B - Condens. Matter Mater. Phys.* **2004**, *70*, 1–3.

[95] **Autonomous high-temperature healing of surface cracks in Al_2O_3 containing Ti_2AlC particles**, L. Boatemaa, M. Bosch, A.S. Farle, G.P. Bei, S. van der Zwaag, W.G. Sloof, *J. Am. Ceram. Soc.* **2018**, *101*, 5684–5693.

[96] **Physical Properties of the MAX Phases**, M.W. Barsoum, in *Encycl. Mater. Sci. Technol. (Second Ed.)*, Elsevier Ltd, **2006**, pp. 1–11.

[97] **Electrical properties of MAX phases**, Y. Medkour, A. Roumili, D. Maouche, L. Louail, in *Adv. Sci. Technol. Mn+1AXn Phases*, Woodhead Publishing Limited, **2012**, pp. 159–175.

[98] **Oxidation behavior of Ti_3AlC_2 at 1000-1400 °C in air**, X.H. Wang, Y.C. Zhou, *Corros. Sci.* **2003**, *45*, 891–907.

[99] **Repeated crack healing in MAX-phase ceramics revealed by 4D in situ synchrotron X-ray tomographic microscopy**, W.G. Sloof, R. Pei, S.A. McDonald, J.L. Fife, L. Shen, L. Boatemaa, A.S. Farle, K. Yan, X. Zhang, S. Van Der Zwaag, P.D. Lee, P.J. Withers, *Sci. Rep.* **2016**, *6*, DOI 10.1038/srep23040.

[100] **On the interactions of Ti_2AlC, Ti_3AlC_2, Ti_3SiC_2 and Cr_2AlC with palladium at 900 °C**, G.W. Bentzel, M. Sokol, J. Griggs, A. Lang, M.W. Barsoum, *J. Alloys Compd.* **2019**, *771*, 1103–1110.

[101] **Theoretical investigation on helium incorporation in Ti_3AlC_2**, J. Xiao, C. Wang, T. Yang, S. Kong, J. Xue, Y. Wang, *Nucl. Instrum. Methods Phys. Res. B* **2013**, *304*, 27–31.

[102] **The Ti3AlC2 MAX Phase as an Efficient Catalyst for Oxidative Dehydrogenation of n-butane**, W.H.K. Ng, E.S. Gnanakumar, E. Batyrev, S.K. Sharma, P.K. Pujari, H.F. Greer, W. Zhou, R. Sakidja, G. Rothenberg, M.W. Barsoum, N.R. Shiju, *Angew. Chem. Int. Ed.* **2018**, *57*, 1485–1490.

[103] **Exfoliation of Titanium Aluminum Carbide (211 MAX Phase) to Form Nanofibers and Two-Dimensional Nanosheets and Their Application in Aqueous-Phase Cadmium Sequestration**, A. Shahzad, M. Nawaz, M. Moztahida, K. Tahir, J. Kim, Y. Lim, B. Kim, J. Jang, D.S. Lee, *ACS Appl. Mater. Interfaces* **2019**, *11*, 19156–19166.

[104] **2D Early Transition Metal Carbides (MXenes) for Catalysis**, Z. Li, Y. Wu, *Small* **2019**, *15*, 1804736.

[105] **Two-dimensional nanocrystals produced by exfoliation of Ti_3AlC_2**, M. Naguib, M. Kurtoglu, V. Presser, J. Lu, J. Niu, M. Heon, L. Hultman, Y. Gogotsi, M.W. Barsoum, *Adv. Mater.* **2011**, *23*, 4248–4253.

[106] **MXenes: An Introduction of Their Synthesis, Select Properties, and Applications**, L. Verger, V. Natu, M. Carey, M.W. Barsoum, *Trends Chem.* **2019**, *1*, 656–669.

[107] **Carbon dioxide adsorption of two-dimensional carbide MXenes**, B. Wang, A. Zhou, F. Liu, J. Cao, L. Wang, Q. Hu, *J. Adv. Ceram.* **2018**, *7*, 237–245.

[108] **Surface Al leached Ti_3AlC_2 as a substitute for carbon for use as a catalyst support in a harsh corrosive electrochemical system**, X. Xie, Y. Xue, L. Li, S. Chen, Y. Nie, W. Ding, Z. Wei, *Nanoscale* **2014**, *6*, 11035–11040.

[109] **Ti_3C_2 MXene as an excellent anode material for high-performance microbial fuel cells**, D. Liu, R. Wang, W. Chang, L. Zhang, B. Peng, H. Li, S. Liu, M. Yan, C. Guo, *J. Mater. Chem. A* **2018**, *6*, 20887–20895.

[110] **25th anniversary article: MXenes: A new family of two-dimensional materials**, M. Naguib, V.N. Mochalin, M.W. Barsoum, Y. Gogotsi, *Adv. Mater.* **2014**, *26*, 992–1005.

[111] **2D metal carbides and nitrides (MXenes) for energy storage**, B. Anasori, M.R. Lukatskaya, Y. Gogotsi, *Nat. Rev. Mater.* **2017**, *2*, 16098.

[112] **Overview of the synthesis of MXenes and other ultrathin 2D transition metal carbides and nitrides**, L. Verger, C. Xu, V. Natu, H.M. Cheng, W. Ren, M.W. Barsoum, *Curr. Opin. Solid State Mater. Sci.* **2019**, *23*, 149–163.

[113] **Effect of Postetch Annealing Gas Composition on the Structural and Electrochemical Properties of Ti_2CT_x MXene Electrodes for Supercapacitor Applications**, R.B. Rakhi, B. Ahmed, M.N. Hedhili, D.H. Anjum, H.N. Alshareef, *Chem. Mater.* **2015**, *27*, 5314–5323.

[114] **H_2O_2 assisted room temperature oxidation of Ti_2C MXene for Li-ion battery anodes**, B. Ahmed, D.H. Anjum, M.N. Hedhili, Y. Gogotsi, H.N. Alshareef, *Nanoscale* **2016**, *8*, 7580–7587.

[115] **Interdiffusion Reaction-Assisted Hybridization of Two-Dimensional Metal-Organic Frameworks and $Ti_3C_2T_x$ Nanosheets for Electrocatalytic Oxygen Evolution**, L. Zhao, B. Dong, S. Li, L. Zhou, L. Lai, Z. Wang, S. Zhao, M. Han, K. Gao, M. Lu, et al., *ACS Nano* **2017**, *11*, 5800–5807.

[116] **TiO_2/MXene Ti_3C_2 composite with excellent photocatalytic CO_2 reduction activity**, J. Low, L. Zhang, T. Tong, B. Shen, J. Yu, *J. Catal.* **2018**, *361*, 255–266.

[117] **2D/2D Heterojunction of Ultrathin MXene/Bi_2WO_6 Nanosheets for Improved Photocatalytic CO_2 Reduction**, S. Cao, B. Shen, T. Tong, J. Fu, J. Yu, *Adv. Funct. Mater.* **2018**, *28*, 1–11.

[118] **$Ti_3C_2T_x$ MXene Catalyzed Ethylbenzene Dehydrogenation: Active Sites and Mechanism Exploration from both Experimental and Theoretical Aspects**, J. Diao, M. Hu, Z. Lian, Z. Li, H. Zhang, F. Huang, B. Li, X. Wang, D.S. Su, H. Liu,

ACS Catal. **2018**, *8*, 10051–10057.

[119] **Reactive metal-support interactions at moderate temperature in two-dimensional niobium-carbide-supported platinum catalysts**, Z. Li, Y. Cui, Z. Wu, C. Milligan, L. Zhou, G. Mitchell, B. Xu, E. Shi, J.T. Miller, F.H. Ribeiro, Y. Wu, *Nat. Catal.* **2018**, *1*, 349–355.

[120] **Plasma technology – a novel solution for CO_2 conversion?**, R. Snoeckx, A. Bogaerts, *Chem. Soc. Rev.* **2017**, *46*, 5805–5863.

[121] **Catalysis Enabled by Plasma Activation of Strong Chemical Bonds: A Review**, P. Mehta, P. Barboun, D.B. Go, J.C. Hicks, W.F. Schneider, *ACS Energy Lett.* **2019**, *4*, 1115–1133.

[122] **Plasma-based conversion of CO_2: current status and future challenges**, A. Bogaerts, T. Kozák, K. van Laer, R. Snoeckx, *Faraday Discuss.* **2015**, *183*, 217–232.

[123] **Methane conversion to higher hydrocarbons in the presence of carbon dioxide using dielectric-barrier discharge plasmas**, C.J. Liu, B. Xue, B. Eliasson, F. He, Y. Li, G.H. Xu, *Plasma Chem. Plasma Process.* **2001**, *21*, 301–310.

[124] **Review of Plasma-Assisted Catalysis for Selective Generation of Oxygenates from CO_2 and CH_4**, S. Liu, L.R. Winter, J.G. Chen, *ACS Catal.* **2020**, *10*, 2855–2871.

[125] **CH_4-CO_2 reforming by plasma - Challenges and opportunities**, X. Tao, M. Bai, X. Li, H. Long, S. Shang, Y. Yin, X. Dai, *Prog. Energy Combust. Sci.* **2011**, *37*, 113–124.

[126] **Plasma-Surface Interactions in Plasma Catalysis**, E.C. Neyts, *Plasma Chem. Plasma Process.* **2016**, *36*, 185–212.

[127] **Use of a non-thermal plasma for the production of synthesis gas from biogas**, V. Goujard, J.M. Tatibouët, C. Batiot-Dupeyrat, *Appl. Catal. A Gen.* **2009**, *353*, 228–235.

[128] **Discharges and Catalysis**, M. Kraus, B. Eliasson, U. Kogelschatz, A. Wokaun, *Phys. Chem. Chem. Phys.* **2001**, *3*, 294–300.

[129] **Understanding plasma catalysis through modelling and simulation - A review**, E.C. Neyts, A. Bogaerts, *J. Phys. D. Appl. Phys.* **2014**, *47*, 224010.

[130] **Removal of Volatile Organic Compounds by Single-Stage and Two-Stage Plasma Catalysis Systems: A Review of the Performance Enhancement Mechanisms, Current Status, and Suitable Applications**, H.L. Chen, H.M. Lee, S.H. Chen, M.B. Chang, S.J. Yu, S.N. Li, **2009**.

[131] **Plasma-catalysis: The known knowns, the known unknowns and the unknown unknowns**, J.C. Whitehead, *J. Phys. D. Appl. Phys.* **2016**, *49*, 243001.

[132] **Dry reforming of methane over a Ni/Al_2O_3 catalyst in a coaxial dielectric barrier discharge reactor**, X. Tu, H.J. Gallon, M. V. Twigg, P.A. Gorry, J.C. Whitehead, *J.*

Phys. D. Appl. Phys. **2011**, *44*, 274007.

[133] **Plasma Catalysis: Synergistic Effects at the Nanoscale**, E.C. Neyts, K. Ostrikov, M.K. Sunkara, A. Bogaerts, *Chem. Rev.* **2015**, *115*, 13408–13446.

[134] **One-Step Reforming of CO_2 and CH_4 into High-Value Liquid Chemicals and Fuels at Room Temperature by Plasma-Driven Catalysis**, L. Wang, Y. Yi, C. Wu, H. Guo, X. Tu, *Angew. Chem. Int. Ed.* **2017**, *56*, 13679–13683.

[135] **Cobalt species and cobalt-support interaction in glow discharge plasma-assisted Fischer-Tropsch catalysts**, J. Hong, W. Chu, P.A. Chernavskii, A.Y. Khodakov, *J. Catal.* **2010**, *273*, 9–17.

[136] **Research on Ni/γ-Al_2O_3 catalyst for CO_2 reforming of CH_4 prepared by atmospheric pressure glow discharge plasma jet**, S. Shang, G. Liu, X. Chai, X. Tao, X. Li, M. Bai, W. Chu, X. Dai, Y. Zhao, Y. Yin, *Catal. Today* **2009**, *148*, 268–274.

[137] **Toluene decomposition using a wire-plate dielectric barrier discharge reactor with manganese oxide catalyst in situ**, Y.F. Guo, D.Q. Ye, K.F. Chen, J.C. He, W.L. Chen, *J. Mol. Catal. A Chem.* **2006**, *245*, 93–100.

[138] **Influence of temperature on gas-phase toluene decomposition in plasma-catalytic system**, V. Demidyuk, J.C. Whitehead, *Plasma Chem. Plasma Process.* **2007**, *27*, 85–94.

[139] **Plasma-assisted methane reduction of a NiO catalyst-Low temperature activation of methane and formation of carbon nanofibres**, H.J. Gallon, X. Tu, M. V. Twigg, J.C. Whitehead, *Appl. Catal. B Environ.* **2011**, *106*, 616–620.

[140] **Combining non-thermal plasma with heterogeneous catalysis in waste gas treatment: A review**, J. Van Durme, J. Dewulf, C. Leys, H. Van Langenhove, *Appl. Catal. B Environ.* **2008**, *78*, 324–333.

[141] **A review of plasma-assisted catalytic conversion of gaseous carbon dioxide and methane into value-added platform chemicals and fuels**, H. Puliyalil, D. Lašič Jurković, V.D.B.C. Dasireddy, B. Likozar, *RSC Adv.* **2018**, *8*, 27481–27508.

[142] **Altering conversion and product selectivity of dry reforming of methane in a dielectric barrier discharge by changing the dielectric packing material**, I. Michielsen, Y. Uytdenhouwen, A. Bogaerts, V. Meynen, *Catalysts* **2019**, *9*, 51.

[143] **Plasma-Catalytic CO_2 Hydrogenation at Low Temperatures**, Y. Zeng, X. Tu, *IEEE Trans. Plasma Sci.* **2016**, *44*, 405–411.

[144] **Plasma-catalytic hydrogenation of CO_2 for the cogeneration of CO and CH_4 in a dielectric barrier discharge reactor: Effect of argon addition**, Y. Zeng, X. Tu, *J. Phys. D. Appl. Phys.* **2017**, *50*, 184004.

[145] **Low temperature catalytic reverse water-gas shift reaction over perovskite catalysts in DBD plasma**, L. Liu, S. Das, T. Chen, N. Dewangan, J. Ashok, S. Xi,

A. Borgna, Z. Li, S. Kawi, *Appl. Catal. B Environ.* **2020**, *265*, 118573.

[146] **Reverse water-gas shift in a packed bed DBD reactor: Investigation of metal-support interface towards a better understanding of plasma catalysis**, Y. Sun, J. Li, P. Chen, B. Wang, J. Wu, M. Fu, L. Chen, D. Ye, *Appl. Catal. A Gen.* **2020**, *591*, 117407.

[147] **Effect of plasma on catalytic conversion of CO_2 with hydrogen over Pd/ZnO in a dielectric barrier discharge reactor**, J. Li, Y. Sun, B. Wang, H. Xiao, J. Wu, L. Chen, M. Fu, D. Ye, *J. Phys. D. Appl. Phys.* **2019**, *52*, 244001.

[148] **Production of CH_4 in a Low-Pressure CO_2/H_2 Discharge with Magnetic Field**, K. Arita, S. Iizuka, *J. Mater. Sci. Chem. Eng.* **2015**, *3*, 69–77.

[149] **Hydrogenation of carbon dioxide to methanol with a discharge-activated catalyst**, B. Eliasson, U. Kogelschatz, B. Xue, L.M. Zhou, *Ind. Eng. Chem. Res.* **1998**, *37*, 3350–3357.

[150] **Atmospheric Pressure and Room Temperature Synthesis of Methanol through Plasma-Catalytic Hydrogenation of CO_2**, L. Wang, Y. Yi, H. Guo, X. Tu, *ACS Catal.* **2018**, *8*, 90–100.

[151] **Highly dispersed Pt-based catalysts for selective CO_2 hydrogenation to methanol at atmospheric pressure**, Y.L. Men, Y. Liu, Q. Wang, Z.H. Luo, S. Shao, Y.B. Li, Y.X. Pan, *Chem. Eng. Sci.* **2019**, *200*, 167–175.